https://doi.org/10.5194/egusphere-2026-6805
Preprint. Discussion started: 11 November 2026
© Author(s) 2026. CC BY 4.0 License.

FES2022 global tide atlas: a step towards SWOT-compliant tidal corrections

Florent H. Lyard[1], Loren Carrère[2], Ergane Fouchet[3], Mathilde Cancet[3], Ramiro Ferrari[3], Mei-Ling Dabat[2], Chafih Skandrani[3], David Greenberg[4], Damien Allain[1], Gérald Dibarboure[5], Nicolas Picot[5]

[1]University Toulouse, CNES, CNRS, IRD, LEGOS, Toulouse, 31400, France
[2]Collecte Localisation Satellites (CLS), Ramonville-Saint-Agne, 31520, France
[3]NOVELTIS SAS, Labège, 31670, France
[4]Bedford Institute of Oceanography, Fisheries and Oceans Canada, Dartmouth, Nova Scotia, Canada
[5]CNES, Toulouse, 31400, France

Correspondence to: Florent H. Lyard (florent.lyard@utoulouse.fr)

Abstract. The FES2022 Global Tide Atlas represents a significant advancement in global tidal modelling, specifically designed to meet the high-resolution tidal correction requirements of modern altimetry missions like the Surface Water and Ocean Topography (SWOT) mission, which demand enhanced resolution and accuracy in the coastal seas. Building on the success of its predecessor FES2014, which performed well in most ocean regions but exhibited residuals issues in coastal, shelf, and polar areas, FES2022 introduces a tenfold increase in mesh resolution, prioritizing coastal and shelf regions. To some extent, this resolution aligns with SWOT's KaRIn instrument capabilities, ensuring compatibility with its high-resolution ocean elevation measurements in shallow water regions. The bathymetry dataset is a composite of GEBCO_2020 and regional patches from other datasets, with a 2-meter depth threshold to better capture shallow coastal dynamics.

The underlying hydrodynamic model (T-UGOm) includes both frequency-domain and time-stepping solvers, with the latter providing more accurate schemes for non-linearities in tides. Bottom friction and wave drag parameters were regionally calibrated. The model also incorporates atmospheric forcing from ERA5 to account for the radiational component of tides when relevant. The data assimilation process uses an ensemble Kalman filter with 358 members, generated by perturbing bathymetry, bottom friction, and wave drag. 16 tidal constituents were assimilated, along with 18 additional waves derived from time-stepping simulations. The assimilation was performed in two iterations (the second one resulting in the final FES2022b atlas) to incorporate the FES2022a Loading and Self-Attraction solution, enhancing the consistency between the model and the observations.

The validation of FES2022b demonstrates substantial improvements over FES2014b and other state-of-the-art models. In the frequency domain, the Root Sum Square (RSS) errors for tidal elevations were reduced to 7.6 mm at altimetry crossovers in the deep ocean, 11.3 mm on shelves, and 42.3 mm at tide gauges compared to FES2014b. Temporal validation showed a variance reduction in Sea Surface Height (SSH) of -2.26 cm² for Jason-3 and -5.75 cm² for AltiKa when compared to FES2014b, with even greater reductions (-16.6 cm² for AltiKa) when compared to GOT4.10c. In polar regions, FES2022b significantly reduced the Sentinel-3A SSH variance in the Arctic (Baffin Bay, Siberian Shelf) and Antarctic (Ross and Weddell

https://doi.org/10.5194/egusphere-2026-6805
Preprint. Discussion started: 11 November 2026
© Author(s) 2026. CC BY 4.0 License.

Seas). Coastal zones benefited from more than 40 cm² of variance reduction within 20 km of the shore. Tidal current validation using 119 current-meter stations showed a 56% improvement compared to FES2014b, with a global RMSD of 2 cm/s for the major axis of tidal ellipses. GRACE gravity field residuals were also reduced, particularly around the Vancouver Island, from 10 cm to 3 cm EWE (Equivalent Water Elevation). Despite these advancements, some local residual errors persist due to bathymetry inaccuracies, shoreline misalignments, and limited high-latitude data coverage. These issues will be addressed in the future FES release.

FES2022 is operational for altimetry de-aliasing corrections and available for download on the AVISO+ website, along with the prediction code on the CNES GitHub. Future improvements will focus on integrating latest bathymetry databases, refining shoreline databases, and enhancing high-latitude coverage of data assimilation through dedicated missions. The model's unprecedented accuracy in coastal and polar regions makes it a recommended replacement for FES2014 in operational and scientific applications.

1 Introduction

Since the early 1990s, several satellite altimetry missions have been monitoring sea level at a global scale, allowing to constitute a long and accurate altimetry database, nearly homogeneous over the entire ocean, and giving access to many regions that were poorly sampled or not sampled at all before the satellite era. Thanks to its current accuracy and maturity, satellite altimetry is now considered as a fully operational observing system dedicated to ocean and climate applications (Escudier et al., 2017). To reach its present accuracy the altimetry system benefits from several geophysical corrections among which the barotropic ocean tide one is the most important in terms of variability. The last version of the Finite Element Solution (FES) global tide model, the FES2014 global ocean atlas released in 2016 (Lyard et al., 2021), was already a significant upgrade compared to previous solutions, thanks to the improvement of both the assimilated data accuracy and the hydrodynamic model performance.

Today, the science and engineering running challenge of making the FES global ocean tidal atlases more accurate and more refined becomes even more complex, especially to satisfy the requirements of the more and more high-resolution and extensive ocean observations from space. Recently, the emergence of modern technologies such as SAR and wide swath altimetry has triggered a renewed interest for coastal (and possibly estuarine) altimetry. In addition, Polar Seas sensitivity to climate change or environmental pressure is drawing tremendous attention. While little progress is to be expected in the deep ocean, where most of the existing tidal atlases perform already quite well (Stammer et al., 2014; Zaron and Elipot, 2020), the FES2022 project has targeted the coastal and shelf seas, and the polar seas, where the modern global atlases still show significant dispersion (as depicted in REF _Ref183004701 \h Figure 1), as its main priorities.

https://doi.org/10.5194/egusphere-2026-6805
Preprint. Discussion started: 11 November 2026
© Author(s) 2026. CC BY 4.0 License.

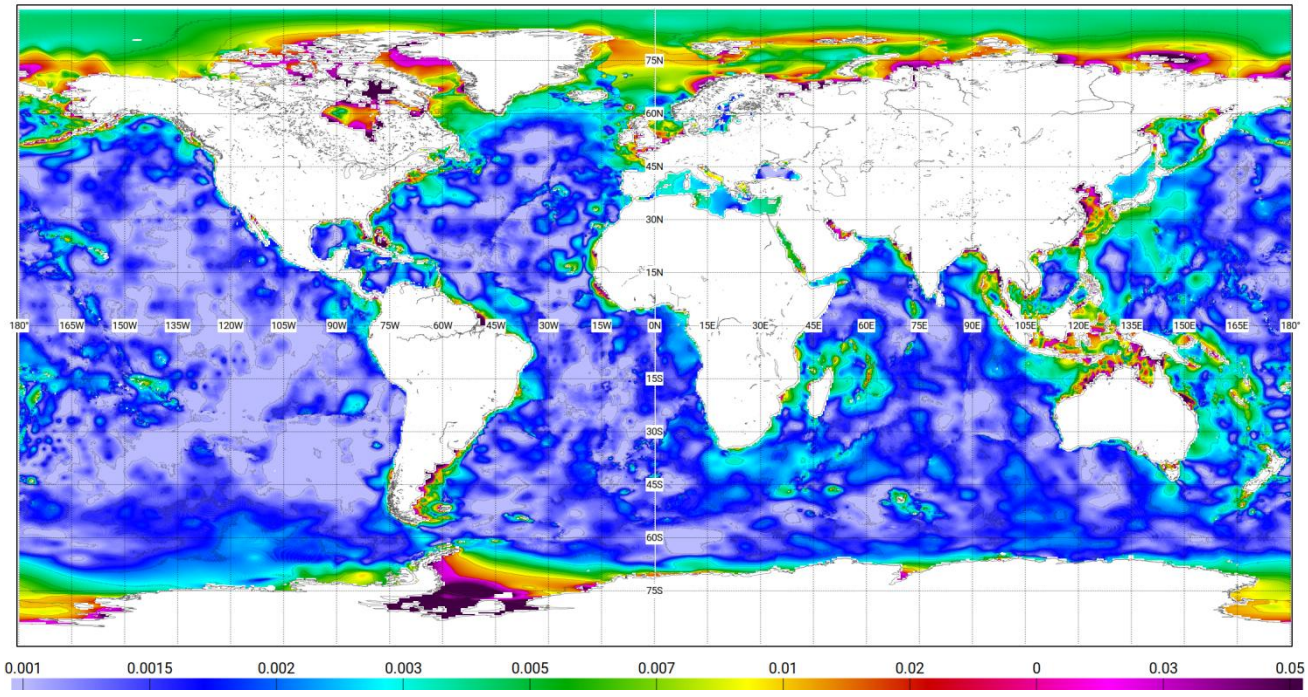


Figure 1: M2 global atlases dispersion from recent models: FES2014, FES2022, GOT4.8, GOT5.5, TPXO8, TPXO9 (in m).

The methodology used in FES2022 is pretty much similar to the one used in FES2014 (Lyard et al., 2021). The main evolutions concern the huge increase in the tidal model mesh resolution, the use of a significantly improved bathymetry database (especially thanks to GEBCO recent releases), and the assimilated data processing. The main driver for mesh evolution has been the new Surface Water and Ocean Topography (SWOT) KaRIn swath altimeter instrument (~140 km wide swath), which delivers high resolution ocean elevation measurements at 2 km resolution (smoothed low-rate product) and 500 m resolution (unsmoothed low-rate product, with a 250 m posting resolution) (JPL, 2025; Morrow et al., 2023). Ideally, the tidal atlas resolution should follow the 500 m SWOT resolution and extend to any coastal details of at least that size. Increased resolution in coastal areas should also be beneficial to the along-track high resolution Synthetic Aperture Radar (SAR) altimetry products in near-shore areas. In practice our choice has been to reach a 4 km along-shore geometrical resolution (i.e., a size of 4 km for the coastal elements' edges) and a 5 km to 10 km mesh resolution on the continental shelves. As a consequence, the FES2022 mesh has about ten times more elements than the FES2014 mesh, and includes many coastal details that were not present in the former version.

For many years, the FES atlases have been selected by space agencies for the operational processing of satellite altimetry de-aliasing corrections. In this context, one of our main objectives for the FES2022 project was to substantially improve the previous FES atlases' accuracy and coverage. As detailed in the next sections, this goal has been globally achieved in the open ocean, shelf seas, and coastal regions. At each project step, i.e., hydrodynamic configuration setup, harmonic data processing, and data assimilation, careful examinations and validations have been performed to monitor the performances. At FES2022

https://doi.org/10.5194/egusphere-2026-6805
Preprint. Discussion started: 11 November 2026
© Author(s) 2026. CC BY 4.0 License.

pre-release step, another round of such investigations has been carried out to qualify the FES2022 atlas. However, and with no surprise, the FES2022 atlas is not free of defects and its performances are not fully homogeneous.

This publication therefore aims to provide comprehensive insights into the modelling components and validation processes, helping FES2022 users make the most effective and informed use of the model regarding their geographic zones and fields of application. The processing of the altimetry and in situ observations for validation and data assimilation is detailed in Sect. 2. Sect. 3 introduces the development of the hydrodynamical tidal solution and the data assimilation in the model is presented in Sect. 4. The tidal atlas assessment and the validation are described in Sect. 5. The model Loading Self Attraction (LSA) is discussed in Sect. 6. Finally, the key results and the perspectives for FES models are summarized in Sect. 7.

Note that complementary to the present publication, some additional information on present and earlier FES global atlases (handbooks), as well as associated prediction software can be found on the AVISO+ website.

2 Tidal harmonic constant data processing

Harmonic data constants derived from both tide gauges (TG) and satellite altimetry have been used for the assimilation and validation of the new FES2022 model. They are described in details in this section and in Appendix A.

2.1 Nadir satellite altimetry observations

Tidal estimates can be obtained through the harmonic analysis of time series of satellite altimetry Sea Level Anomalies (SLA). The accuracy of the altimetry-derived tidal estimates firstly depends on the missions' orbit parameters and duration, which determine the level of contamination of the tidal estimation by other ocean signals. It also depends on the quality of the altimeter standards applied. Compared to the previous model FES2014, FES2022 benefits from significantly longer times series on the reference mission orbits, and from new high latitude missions.

The reference mission orbits here are those of the Topex/Poseidon-Jason suite on its 10-day nominal orbit (TP-J1-J2-J3 hereinafter) and on its 10-day interleaved orbit (TPN-J1N-J2N). However, the orbit inclination of the Topex/Poseidon-Jason suite being 66°, other missions with less favorable configurations for tidal estimates must be considered in the high latitudes.

In the end, three different altimeter datasets have been constructed for the purpose of the study: along-track data, crossovers, and boxes for high latitudes.

2.1.1 Altimetry data processing details

The global ocean Sea Surface Height (SSH) observations come from the DT2021 reference dataset, that is the Delayed Time (DT) Level-3 altimeter satellite along-track data reprocessed in 2021, and distributed by the EU Copernicus Marine Service (EU Copernicus Marine Service, 2022; Faugère et al., 2022). This database contains measurements homogeneously processed and corrected for the 13 altimeter missions that have flown for 28 years, since 1992: Topex/Poseidon (TP), ERS1, ERS2, GFO,

https://doi.org/10.5194/egusphere-2026-6805
Preprint. Discussion started: 11 November 2026
© Author(s) 2026. CC BY 4.0 License.

Jason-1 (J1), Envisat (EN), Jason-2 (J2), Cryosat-2 (C2), AltiKa (AL), HY-2A, Jason-3 (J3), Sentinel-3A (S3A), and Sentinel-3B (S3B).

The long-term altimeter series used to compute the FES2022 dataset are described in Table 1. The multi-mission long-term series like TP-J1-J2-J3 and TPN-J1N-J2N cover longer timespans than in the previous tidal solution FES2014, with the addition of the J3 mission, as well as a few new cycles from J2N.

The estimation of altimetry-derived tidal estimates starts with the computation of the along-track altimeter SLA defined by Eq. (1).

$$SLA = Orbit - Range - Instrumental\ corrections - Geophysical\ corrections - Mean\ Profiles\ (or\ MSS) - Orbit\ correction \quad (1)$$

The instrumental corrections are the wet tropospheric correction, the dry tropospheric correction, the ionospheric correction and the Sea State Bias (SSB) correction. The geophysical corrections are the Dynamic Atmospheric Correction (DAC) and the tidal corrections, i.e., the geocentric tide, the solid earth tide, the polar tide, and the internal tides. Up-to-date instrumental and geophysical corrections are considered for each mission (see Fig. A1 in Appendix A, and Faugère et al. (2022) for the details). Most corrections are new compared to the data used for FES2014. In particular the FES2014b geocentric tide correction (i.e., ocean and loading tide components) is used (Lyard et al., 2021).

The loading tide correction is applied to the altimeter measurements in order to extract only the ocean tide component for the computation of the ocean tidal atlases. An iterative process similar to the one used for FES2014 has been followed. In a first step, the FES2014 tidal loading model was applied. The resulting altimetry data have been used in the data assimilation process to produce a preliminary version of the ocean tide model, noted FES2022a (not distributed). Based on this FES2022a ocean tide atlas, a tidal loading atlas was computed and used to produce a second version of the altimeter datasets that was assimilated into the final version of the ocean tide model, named FES2022b.

An orbit error correction is applied for all missions. This correction, which rescales the missions on a more precise reference mission (TP-J), allows reducing the error budget of the data while reducing the residual orbit error, hence increasing the signal to noise ratio of the tide estimation and reducing the associated error for non-reference missions.

The Mean Profiles (MP) of Sea Surface Height (SSH) are computed along each repetitive satellite track over a given period. Within the DUACS-2021 reprocessing context, new MP have been computed using the new DT-2021 database described above and considering the 20-year reference period 1993-2012. Note that the accuracy of the MPs strongly decreases in very high latitude regions due to the lack of measurements (seasonal ice cover). For the cases where the MP cannot be computed (like geodetic missions characterized by a drifting orbit, such as JasonX-G, and AltiKa-G, or CryoSat-2 that has a very long cycle) or is not accurate enough yet (S3-B), we use the CNES_CLS_2022 Mean Sea Surface (MSS) described in Schaeffer et al. (2023) to compute the SLA.

https://doi.org/10.5194/egusphere-2026-6805
Preprint. Discussion started: 11 November 2026
© Author(s) 2026. CC BY 4.0 License.

To obtain tidal estimates as accurate as possible, the satellite altimetry SLA are then processed to further improve the signal to noise ratio before performing the harmonic analysis, with some dedicated approaches for internal tides, and for K1 and S2 frequencies. Details are provided in Appendix A.

Mission	Start date	End date	Start cycle	End cycle	Total number of cycles
TP-J1-J2-J3					
TP	31/12/1992	24/04/2002	11	353	1002 (743 for FES2014)
J1	24/04/2002	19/10/2008	11	249	
J2	19/10/2008	26/05/2016	11	290	
J3	26/05/2016	19/09/2020	11	169	
TPN-J1N-J2N					
TPN	16/09/2002	08/10/2005	369	481	244 (223 for FES2014)
J1N	10/02/2009	03/03/2012	262	374	
J2N	13/10/2016	03/04/2017	305	322	

Table 1: Timespan of each altimeter missions used for the FES2022 altimeter database

2.1.2 Tidal harmonic analysis

To retrieve the residual tidal harmonic constants from the altimetry SLA time series, a harmonic analysis is performed. Then, the ocean tide model used to correct the altimetry SLA (FES2014b in our case) is added to these residual tidal harmonics, in order to obtain the full tidal harmonics. In addition to the along-track SLA dataset, an altimetric crossover database was computed, considering measurements on both the ascending and the descending tracks at the crossover locations. This allows doubling the temporal sampling of the time series and thus improves the tidal estimations (Lyard et al., 2021). We finally obtained two along-track datasets and two crossover datasets, for TP-J1-J2-J3 and TPN-J1N-J2N.

In addition to these global datasets, a specific processing is done for the high latitudes. Indeed, the reference altimeter TP-Jason suite only samples latitudes until 66° but many other altimeters are sampling higher latitudes (Table 2). Although these non-reference missions have a higher error budget and bad tide-aliasing properties (see Table 1 in Cancet et al., 2025), some recent studies (Carrere et al., 2019) have shown that gathering the altimetry observations in boxes, instead of processing the data along the tracks, significantly improves the quality of the tidal estimates, as the aliasing periods are reduced.

Mission	Cycle (days)	Min/max latitudes	Sun-synchonous	Cycles used	Start date	End date
S3A	27	+/-81.5	yes	1-63	01/03/2016	11/10/2020

https://doi.org/10.5194/egusphere-2026-6805
Preprint. Discussion started: 11 November 2026
© Author(s) 2026. CC BY 4.0 License.

S3B	27	+/-81.5	yes	19-44	27/11/2018	21/10/2020
C2	29 (sub cycle)	+/-88	no	1-134	16/07/2010	05/05/2020
AL / ALG	35 / EoL	+/-81.5	yes	1-22/ 23-142	14/03/2013	17/08/2020
HY2A/ HY2AG	14 / EoL	+/-81	yes	66-117/ 118-288	12/04/2014	09/06/2020
ENVISAT/ ENN	35 / EoL	+/-81.5	yes	6-93/ 94-113	14/05/2002	08/04/2012
ERS1	35	+/-81.5	Yes	15-27/ 30-40	23/10/1992/ 10/04/1994	20/12/1993/ 21/03/1995
ERS2	35	+/-81.5	Yes	1-74	15/05/1995	14/05/2002
GFO	17	+/- 72	no	37-222	07/01/2000	07/09/2008

Table 2: Parameters and cycles used for the high-latitude missions in the FES2022 database. EoL stands for End-of-Life missions.

The timespan of the missions used to compute the high latitude FES2022 database are described in Table 2. The along-track SLAs from all available missions have been combined in 1° by 1° boxes to build time series, and the harmonic analysis was performed in each box. The analysis spectrum is optimized for non-regular sampling (due to seasonal ice-cover notably), considering the correlation between the tidal waves within the harmonic matrix.

For altimetry series characterized by mission-specific aliasing and wave separation problems as described before, the analyzed spectrum (see Table 3) was adapted according to the missions and recording lengths, following the Rayleigh criterion: for TP-J1-J2-J3 data (along-track and crossover points), a spectrum of 44 waves has been analyzed. This spectrum corresponds to the characteristic waves on the continental shelves.

Notice that some minor tides have also been estimated, such as J1, OO1, and MP1, following Ray (2019). J1 (Fig.2) and OO1 (not shown) have amplitudes stronger than 1-2 cm locally with global coherent patterns except some noise visible mostly in southernmost latitudes and in the northern Atlantic Ocean. Estimated MP1 (not shown) has a very weak and noisy pattern on the global ocean.

Due to wave separation problems, the number of waves analyzed for the TPN-J1N-J2N data is reduced to 22. This spectrum corresponds to waves representative of the deep ocean. For the high-latitudes boxes, a reduced spectrum of 9 main waves is used.

Analyzed altimetry datasets	**Analyzed tidal waves**			
	Diurnal	**Semi-diurnal**	**Compound**	**Long period**

https://doi.org/10.5194/egusphere-2026-6805
Preprint. Discussion started: 11 November 2026
© Author(s) 2026. CC BY 4.0 License.

TP-J1-J2-J3 (along-track and crossovers)	K1, O1, P1, Q1, Psi1, Sigma1, Ki1, Phi1, Theta1, Pi1, J1, OO1, MP1	M2, N2, S2, K2, 2N2, Nu2, Mu2, L2, T2, R2, Lambda2, E2	M4, MS4, M3, M6, MN4, 2MS6, 2SM2, MK4, M_SK_2, MSK2, N4, M_KS_2, 2MK6, 2SM6, MKS2, S4	Mf, Mm, Mtm, MSqm, MSf, MStm
TPN-J1N-J2N (along-track and crossovers)	K1, O1, P1, Q1	M2, N2, S2, K2, 2N2, Nu2, Mu2, L2, T2, R2	M4, MS4	Mf, Mm, Mtm, MSqm, MSm
High-latitude boxes	K1, O1, P1, Q1	M2, N2, S2, K2, 2N2	/	/

Table 3: Tidal spectrum analyzed for each type of altimetry dataset, decomposed in tidal wave types.

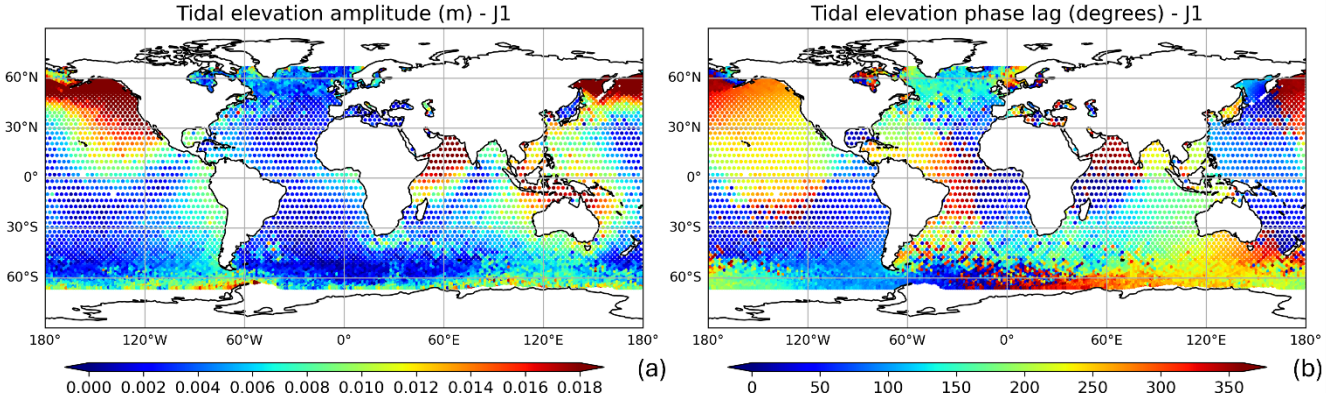


Figure 2: (a) Amplitude (in meters) and (b) phase lag (in degrees) of the minor tide J1 estimated at TP-J1-J2-J3 crossovers.

2.1.3 Accuracy and availability of altimetry data

Thanks to the better altimeter corrections used in the database and to the longer time series available, the FES2022 altimetry dataset benefits from a better overall accuracy and availability of data, including in coastal regions, compared to the FES2014 dataset (see Fig. A2 in Appendix A). In particular, about twice more TPN-J1N-J2N crossover estimations are available for FES2022 (Table 4). The signal-to-noise values for the tidal estimates at the TP-J1-J2-J3 crossovers are significantly improved, compared to FES2014 (Table 5), and the mean differences between TP-J1-J2-J3 tidal estimations on ascending and descending tracks are only 5 mm on global ocean for the main semi-diurnal waves and 8 mm for K1 (Table 6). Along-track estimations using TPN-J1N-J2N are improved compared to FES2014, but differences at crossovers remain twice higher than for the reference orbit (10 mm for the semi-diurnal waves and 17 mm for K1). The signal-to-noise value is also significantly increased when using the TPN-J1N-J2N crossovers compared to along-track estimations, which indicates the better quality of the crossover dataset.

https://doi.org/10.5194/egusphere-2026-6805
Preprint. Discussion started: 11 November 2026
© Author(s) 2026. CC BY 4.0 License.

	TP-J1-J2-J3	TPN-J1N-J2N
FES2022	9034	6392
FES2014	8425	3166

Table 4: Number of estimations at crossovers considering long-term altimeter series for the FES2022 and the FES2014 datasets.

	M2	K1	S2	N2
FES2022	218	69	87	53
FES2014	118	32	43	27

Table 5: Signal to noise (S/N) values for TP-Jason crossover estimates of the main tidal components for the FES2022 and FES2014 datasets, averaged over the global ocean. S/N=amplitude/background noise, with the background noise defined as the residual spectral energy around tidal frequencies (Ponchaut et al., 2001).

ASC - DESC	M2	K1	S2	N2	RSS
TP-J1-J2-J3	0.5	0.8	0.5	0.4	1.1
TPN-J1N-J2N	1.0	1.7	1.0	0.9	2.4

Table 6: Mean complex difference (in cm) between ascending and descending along-track estimations for the TP-J1-J2-J3 and TPN-J1N-J2N missions, for the waves M2, K1, S2, and N2. Only regions with an ocean variability lower than 225 cm² are considered here.

2.2 In situ tide gauge data

The validation and assimilation of FES tidal models require accurate in situ data. The tide gauge databases collected for previous global models (FES2012 and FES2014, Lyard et al., 2021) have been updated with tide gauge stations from the UHSLC database (Caldwell et al., 2015; https://uhslc.soest.hawaii.edu/data/?rq) and the EMODnet platform (https://emodnet.ec.europa.eu/geonetwork/srv/eng/catalog.search#/metadata/5d3feda8-2a38-4301-9300-0f16f0d3762d).

The tidal signal can be accurately retrieved from the tide gauge sea surface height observations provided that time series have a high frequency (preferably less than one hour) and a duration of minimum of three months. Some quality check was applied to the tide gauge time series to eliminate outliers (spikes) and identify potential data gaps and drifts. These criteria are necessary to ensure the good performance of the harmonic analysis. The tidal constituents retrieved from the tide gauge time series were validated against the FES2014 global tidal model and against the nearby stations to identify possible major inconsistencies due to remaining issues in the tide gauge data. The final global database consists of 1464 tide gauges (Figure 3). However, the available tidal spectrum varies depending on the station, as some data come from databases or scientific papers that only provide tidal harmonic constituents for a limited number of components (no time series publicly available).

https://doi.org/10.5194/egusphere-2026-6805
Preprint. Discussion started: 11 November 2026
© Author(s) 2026. CC BY 4.0 License.

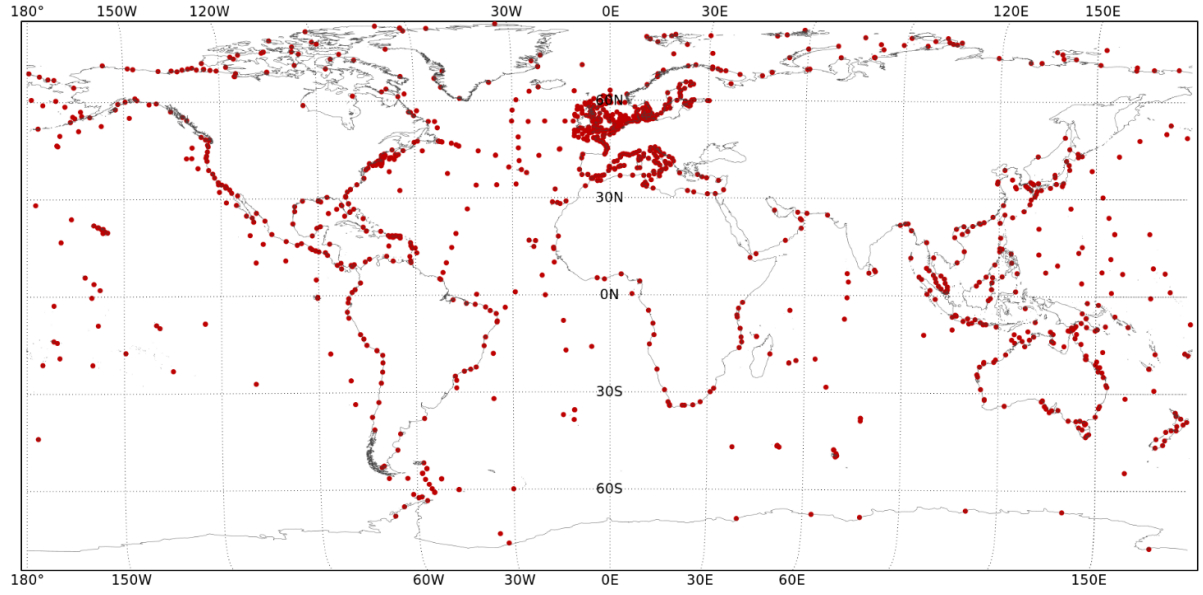


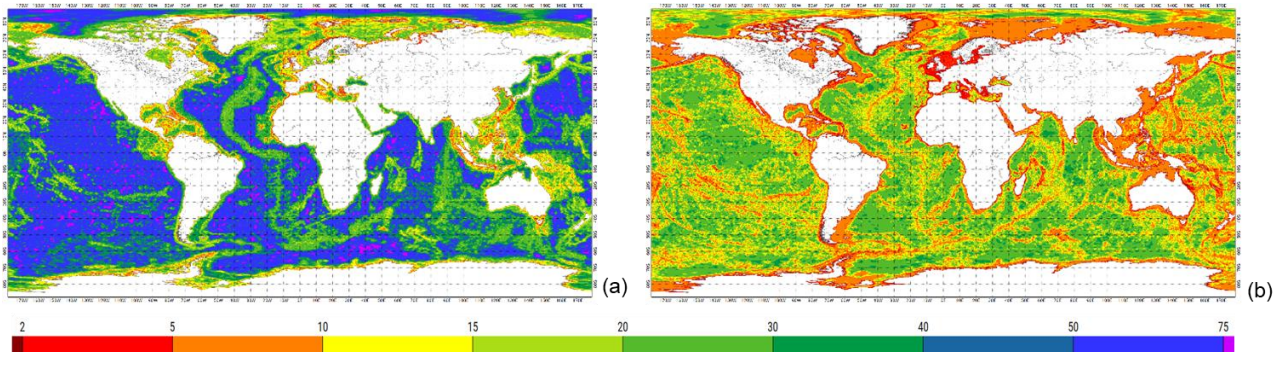
Figure 3: Location of the tide gauges in the FES2022 database

3. Hydrodynamic prior solutions

As in earlier releases of FES atlases, great attention and efforts have been paid to guarantee the best possible accuracy of the prior (to data assimilation) solutions. Besides usual model inputs and setting preparation, the unstructured model grid has been dramatically upgraded to anticipate the needs of the SWOT mission in terms of precise and accurate coastal corrections.

3.1 Unstructured mesh design

The objectives of the mesh upgrade (starting from the FES2014 mesh) were firstly to increase resolution in all regions (Figure 4), with a special effort on along shore/shelf resolution, and to cover most of the coastal details in the global ocean, while keeping a workable configuration, i.e., with workable computational and archiving costs.



https://doi.org/10.5194/egusphere-2026-6805
Preprint. Discussion started: 11 November 2026
© Author(s) 2026. CC BY 4.0 License.

Figure 4 : FES unstructured mesh resolution (kilometers) for FES2014 (a) and FES2022 (b)

The deep ocean resolution standard target has been set to about 25 km, the shelf break resolution standard target to 5 km, the on-shelf standard target to 10 km, and the alongshore standard target to 4 km. In practice, the mesh generation results in an effective resolution that is higher than or equal to the target resolution. The mesh resolution is governed by several depth-dependent criteria, including geometry and alongshore resolution. The most demanding criterion is the depth gradient, which is expressed with Eq. (2).

$$l = 0.4 * \frac{H}{\|\nabla H\|} \quad (2)$$

where H is the local bathymetry and l the corresponding element size.

In standard meshing, we restrict the action of this criterion to regions deeper than 200 m. This limitation does not jeopardize the increase of resolution needed on shelf breaks (necessary to the precise internal tide stress parameterization), while avoiding massive mesh over-densification on the shelves and in coastal areas. For the latter, it might result in over-smoothed tidal currents at some locations, however with a limited effect on tidal elevation accuracy (our main objective). As mentioned later in this section, this strategy was then reconsidered at least in some places of special interest.

Shorelines have been extracted from the GSHHG v2.3.7 database (Wessel and Smith, 1996), and processed to eliminate isolated details (islands, river mouths, etc..) below the resolution target and to aggregate sub-resolution islands that form macro-obstacles together. In post-production diagnostic studies, we noticed that the GSHHG dataset contains some significant errors (from a few hundred meters up to 20 km or more) in many places: shifts in the shoreline position, seasonal sea ice/open ocean limits taken as shorelines, etc. These anomalies disrupt the mesh coastal extent, but also introduce some inconsistencies with the bathymetry dataset, which affect the model accuracy in some very coastal areas (e.g., Tierra del Fuego, Chile; Frobisher Bay, Labrador Sea).

In some places, the mesh resolution has been specifically increased beyond 4 km, like in some narrow straits (Gibraltar, Bosporus, etc.), or for islands of size close to the targeted alongshore resolution, for which a local sub-sampling distance has been used to properly discretized their limits. In a final step, a call has been addressed to the science and hydrographic services community to offer them the possibility to suggest places of interest where higher (than FES2022-standard) resolution could be desirable. Among the several answers we received, the Great Barrier Reef is an excellent illustration (Figure 5), as not only has the resolution been increased (2 km alongshore, 7.5 km on shelf), but the reef topography gradients have also been taken into account (i.e., the depth gradient resolution criterion has been activated over the reefs), resulting in locally increased resolution between 1 and 2 km.

https://doi.org/10.5194/egusphere-2026-6805
Preprint. Discussion started: 11 November 2026
© Author(s) 2026. CC BY 4.0 License.

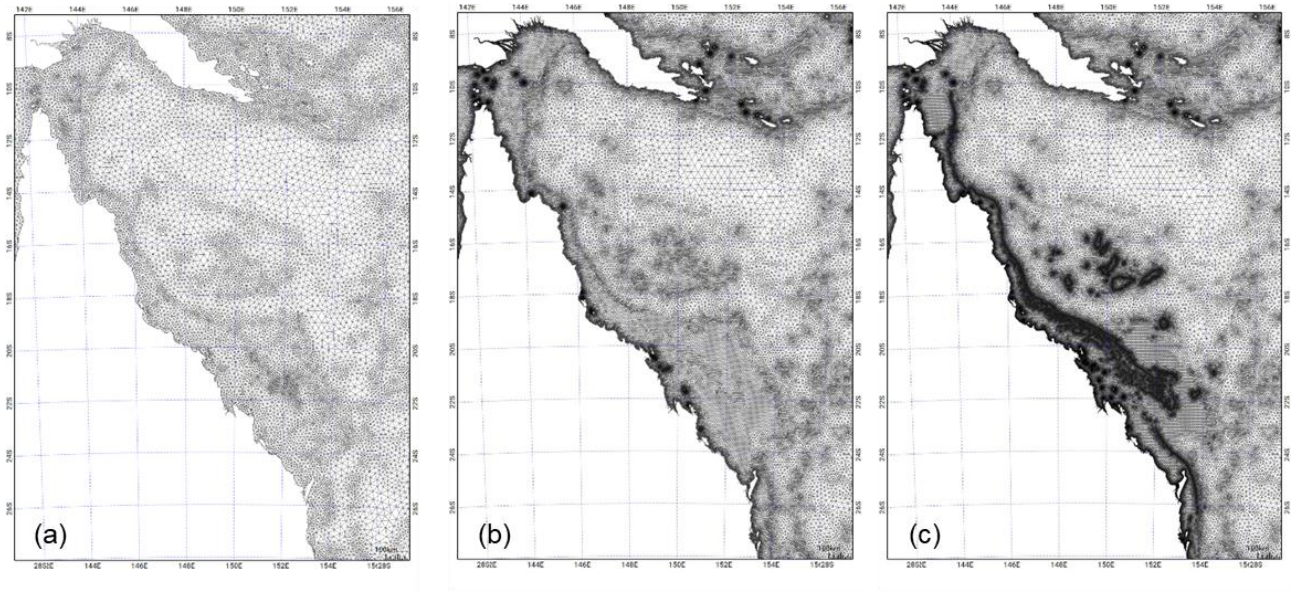


Figure 5: Mesh over the Great Barrier in Australia: FES2014 (a), FES2022-standard upgrade (b), FES2022-focused upgrade (c)

The overall increase in resolution in the Great Barrier region corresponds to about 130 000 elements, i.e., about 1 % of the final FES2022 mesh size. A similar refinement has been done for the New-Caledonian lagoon (semi enclosed in a reef barrier) with an overhead of about 45 000 elements. These numbers show that systematically triggering the depth gradient criterion in shallow water in a global ocean mesh would increase the number of elements above workable values.

In conclusion, the FES2022 mesh has been constructed in about 90 iterations (mostly regional/coastal ones, plus the regions of interest) before completion. The final number of elements is about 11 000 000, nearly ten times larger than for the FES2014 mesh. This is a considerable gain in resolution, which has demanded significant efforts to numerically optimize the hydrodynamic, assimilation and pre/post-processing software.

3.2 FES2022 hydrodynamic (prior) solutions

The FES2022 hydrodynamic solution was computed using the T-UGOm model as for FES2014 atlas (Lyard et al., 2021). T-UGOm has a dual tidal solver implementation, one based on frequency-domain (FD) tidal equation, and one based on time-stepping (TS) shallow-water equations coupled to a built-in harmonic analysis module. The frequency-domain solver is quasi-linearized, i.e., it solves most but not all of the non-linear bottom friction effects through iteratively adjusted parameterization (Le Provost and Vincent, 1986). It has however a much smaller computational cost than the time-stepping approach and is thus preferably used to generate the ensemble members needed for data assimilation. The time-stepping solver has naturally more accurate non-linear schemes and is preferred to generate atlas solutions that will not go through the data assimilation optimization. In both cases, the accuracy of the hydrodynamic solutions is critical. This is obviously true for non-assimilated solutions but not only, as data assimilation always performs better when the prior solution is closer to the observational sea

https://doi.org/10.5194/egusphere-2026-6805
Preprint. Discussion started: 11 November 2026
© Author(s) 2026. CC BY 4.0 License.

truth. The FD and TS configurations are calibrated separately mostly because of the internal wave drag parametrization. This parameterization is straight forward for the FD solver, but relies on stronger arbitrary assumptions in the TS solver (Lyard et al., 2021).

3.2.1 Model parameters

Model bathymetry: as with our previous FES releases, the bathymetry dataset from which the model depths at numerical nodes are computed is a composite product. In the FES2022 case, the GEBCO_2020 bathymetry dataset (GEBCO Compilation Group, 2020; https://www.gebco.net/data_and_products/gridded_bathymetry_data/gebco_2020) has been chosen to initiate the combination process. Compared to previous GEBCO datasets, GEBCO_2020 showed significant accuracy improvements. A sequence of patches has been applied to the GEBCO dataset to include the most up-to-date regional datasets available at that time. As the GEBCO_2020 dataset did not include the data needed to derive the free water thickness in Antarctica ice-shelf cavities, we used the RTOPO-2.0.1 dataset (Schaffer and Timmermann, 2016) in these areas. Regional patches have also been applied from US Coastal Relief (NOAA National Centers for Environmental Information, 2023), EMODnet (EMODnet Bathymetry Consortium, 2020; https://emodnet.ec.europa.eu/en/bathymetry), Great Barrier dataset (Beaman, 2020), New-Caledonian Shom/IRD dataset (Shom-IRD, 2021), BedMachine Greenland v3 (Morlighem et al., 2017a, 2017b), and JODC J-EGG500 data set for Japan (JODC, https://www.jodc.go.jp/jodcweb/JDOSS/infoJEGG.html). The SRTM15 2.1 dataset (Tozer at al., 2019) has been used for patching the Bering strait and Siberian shelf bathymetry. The Hudson Bay and Amazon estuary bathymetries were also updated by using depth sounding (respectively extracted from CHS NONNA bathymetry products [https://open.canada.ca/data/en/dataset/d3881c4c-650d-4070-bf9b-1e00aabf0a1d], and F. Durand personal communication). Despite our efforts, the overall quality of the composite bathymetry database remains extremely heterogeneous, and the FES2022 solutions accuracy in coastal regions can be strongly impacted by the local bathymetry accuracy.

Finally, the bathymetry threshold that aims to smooth out unrealistic features of the bathymetry in the very shallow water regions in the model was set to 2 m (versus 10 m for FES2014), which means that more confidence was put in the shallow bathymetry.

Barotropic tides dissipation parameters: The dissipation in the model is mainly driven by the bottom friction (BF) and by the energy transfer from the barotropic mode to the baroclinic mode, called wave drag (WD) hereinafter. These two parameters have been fine-tuned in FD mode, testing over 30 combinations and ensuring the improvements in one region did not degrade the accuracy elsewhere. Global values were determined ($1.25\ 10^{-3}$ m for the BF, 27.5 for the WD), and Table 7 and Table 8 respectively show the regional BF and WD values that finally provided the best compromise for all the tidal waves in the deep ocean and on the shelves, relative to tide gauge and altimetry observations.

For the simulation in TS mode, the parameterization is simplified, with a unique global value of BF (0.003 m) and WD (50).

https://doi.org/10.5194/egusphere-2026-6805
Preprint. Discussion started: 11 November 2026
© Author(s) 2026. CC BY 4.0 License.

Table 7: Optimal roughness length (m) per region.

	Patagonian shelf	Weddell Sea	Amazon shelf	Gulf of St. Lawrence	Hudson Bay	North East Atlantic	Svalbard
roughness length (m)	0.0015	0.0035	0.0001	0.00125	0.002	0.0025	0.00125

	White Sea	Sea of Okhotsk	Yellow Sea	North Australia	Bering Sea	South China Sea	Gulf of Alaska
roughness length (m)	0.002	0.0035	0.0001	0.0005	0.00025	0.00025	0.00125

Table 8: Optimal wave drag coefficient per region.

	Arctic	Med. Sea	North Atlantic	North Pacific	South Atlantic	South Indian	South Pacific	Tropical Atlantic	Tropical Indian	Tropical Pacific
WD	27	29	29.5	29.5	29.5	27	27	29	28	27.5

Loading and Self Attraction (LSA) forcing: The FES2014 LSA solution has been used for the computation of the FES2022a FD hydrodynamic solution and all the ensemble simulations. In a second step, the FES2022a LSA computed from the FES2022a assimilated tidal model was used to generate a new version of the FD hydrodynamic solution, which was assimilated to produce the final FES2022b atlas. The validation results presented in the next section correspond to the FD simulation based on the FES2022a LSA solution. For the TS hydrodynamic simulations, only the FES2022a LSA forcing was used.

Atmospheric forcing: To take into account the dual nature of the S2 tidal component (gravitational and radiational), dedicated atmospheric forcing has been used in the FD simulation. The atmospheric surface pressure S2 (in harmonic form) has been computed from the ERA5 atmospheric mean sea level pressure, over a period spanning the assimilation data acquisition time (1993-2020). The TS simulations have been forced with the hourly ERA5 pressure at sea level and wind at 10 m (Hersbach et al., 2023; Hellerman and Rosenstein, 1983).

TS simulations have been performed over a period of almost two years (01/2007-11/2008, arbitrarily chosen) to accurately harmonically analyze the non-linear and minor tidal waves. The TS simulation without atmospheric forcing was run to extract long-period and astronomical compound tidal components. The TS simulation with atmospheric forcing was done to obtain the S1 and the annual (Sa) tidal components (mainly radiational) and thus ensure compatibility between the tidal corrections and the Dynamic Atmospheric Correction for satellite altimetry sea surface height observations.

https://doi.org/10.5194/egusphere-2026-6805
Preprint. Discussion started: 11 November 2026
© Author(s) 2026. CC BY 4.0 License.

3.2.2 Prior solutions assessment

The hydrodynamic solutions (in FD and TS modes) have been validated against the tide gauges and altimetry datasets presented in Sect. 2, and compared with the FES2014 prior and assimilated solutions. The diagnostics have been computed for all the tidal waves, separating altimetry cross-over points in the deep ocean (depths over 500 m) and in shelf areas (depths below 500 m). Table 9 summarizes the results for the 7 main components (M2, S2, K1, O1, K2, N2, and Q1) and provides the Root Sum Square (RSS) estimated over these components. The FES2022 FD hydrodynamic atlas shows smaller misfits to observations for each tidal constituent, compared to the FES2014 FD hydrodynamic solution. As expected, the improvements are of limited magnitude for the deep ocean. They are much more significant on the shelves, with a total RSS reduction of 37.2 mm from FES2014 FD hydrodynamic to FES2022 FD hydrodynamic. This result is mostly due to the improvements on the M2 tidal constituent, and on the semi-diurnal waves in general, while the results on the diurnal waves are more contrasted. Similar results are obtained when comparing to the tide gauge database.

Table 9 : Global comparison of FES2014 FD hydrodynamic, FES2022 FD and TS hydrodynamic (with FES2022 LSA forcing) and assimilated FES2014b solutions: vector differences (mm) against the deep (top table) and shelf (middle table) altimetry crossover points, and the tide gauge dataset (bottom table)

		M2	K1	S2	O1	K2	N2	Q1	RSS
XOVERS DEEP	FES2014 hydrodynamic FD	15.5	8.6	8.4	6.0	4.9	4.4	3.4	21.8
	FES2014b	3.2	3.2	3.1	2.6	3.8	2.4	2.8	8.4
	FES2022 hydrodynamic FD	13.1	6.8	7.7	4.7	4.3	4.0	3.0	18.5
	FES2022 hydrodynamic TS - no atmosphere (*except S2)	15.1	7.0	7.9*	4.5	4.3	4.1	2.9	20.1
XOVERS SHELF	FES2014 hydrodynamic FD	114.2	27.8	28.6	19.6	11.3	21	5.5	125.0
	FES2014b	22.1	7.7	9.7	4.9	4.5	5.4	4.5	27.6
	FES2022 hydrodynamic FD	74.6	27.3	25.2	19.2	9.1	16.6	5.8	87.8
	FES2022 hydrodynamic TS- no atmosphere (*except for S2)	68.4	28.7	23.5*	19.3	9.0	14.2	5.7	82.1
TIDE GAUGES	FES2014 hydrodynamic FD	121.2	39.3	45.1	33.6	16.7	25.2	8.2	142.8
	FES2014b	81.4	17.3	33.3	13.6	10.6	17.9	5	93.4
	FES2022 hydrodynamic FD	83.6	25.3	34.1	17.3	11.3	19.1	5.2	98.0
	FES2022 hydrodynamic TS- no atmosphere (*except for S2)	85.1	25.5	36.3*	20.1	12.9	19.4	5.5	100.9

https://doi.org/10.5194/egusphere-2026-6805
Preprint. Discussion started: 11 November 2026
© Author(s) 2026. CC BY 4.0 License.

The comparison between the FES2022 TS and FD simulations for the main tidal waves generally shows close vector differences. Slight degradations are observed for the TS simulation on M2 (2 mm for deep crossover points and 1.5 mm for tide gauges) but the improvement on shelf crossover points (6.2 mm) suggests that TS compound tidal waves build on more accurate linear waves than spectral ones on the continental shelves.

In summary, Table 9 demonstrates that the FES2022 hydrodynamic model (in TS and FD modes) shows significant improvements over the FES2014 hydrodynamic model, and, although not constrained by any observation, remarkably reduces discrepancies relative to the assimilated FES2014b model.

4 Data assimilation

The data assimilation methodology used for the production of the FES2022 atlas is the same as for the FES2014 atlas, described in Lyard et al. (2021). In short, it relies on the ensemble Kalman Filter, in a formulation based on the use of representer functions for the observations (Bennett and McIntosh, 1982; Bennett, 1992) to solve for the optimal problem. Representer functions are derived from the model error covariances (Lyard, 1999) and somehow define the domain of influence of the observations. Model error covariances are approximated from the ensemble covariances of members using stochastic modelling, based on the perturbation of one or more model parameters. The data assimilation is conducted directly in the frequency domain, for each tidal component separately. The ensemble of perturbations is designed to ensure that the mean of the ensemble of simulations closely aligns with the FES2022 reference hydrodynamic simulation.

4.1 Ensemble construction

Ensemble simulations are computed by regionally altering the wave drag and bottom friction coefficients around the reference values, as well as changing the bathymetry, in regions where the model is most sensitive to such alterations. The bathymetry perturbations have been generated in the same regions as for the FES2014 ensemble (see Fig. 8 in Lyard et al., 2021), using global bathymetry datasets: RTopo-1.0.5b (Timmerman et al., 2010) and ALBMAPv1 (Le Brocq et al., 2010) in the Antarctic Ocean, GEBCO2014 (Weatherall et al., 2015) and SRTMplus-v1.2 (Becker et al., 2009) elsewhere. The bathymetry threshold was also set to four different values for each perturbated region (2, 4, 6, and 10 meters). The complete ensemble of perturbations (wave drag, bottom friction and bathymetry) comprises 358 simulation members, for each tidal constituent. As an illustration of the ensemble dispersion, the RMS of the ensemble simulations for M2 and K1 amplitudes are displayed on Figure 6. The data assimilation process will more significantly constrain the model in the regions with high ensemble member variability. In regions with low variability among ensemble members, particularly in the deep ocean, the data assimilation system will rely more heavily on the prior hydrodynamic solution with higher confidence in its accuracy.

https://doi.org/10.5194/egusphere-2026-6805
Preprint. Discussion started: 11 November 2026
© Author(s) 2026. CC BY 4.0 License.

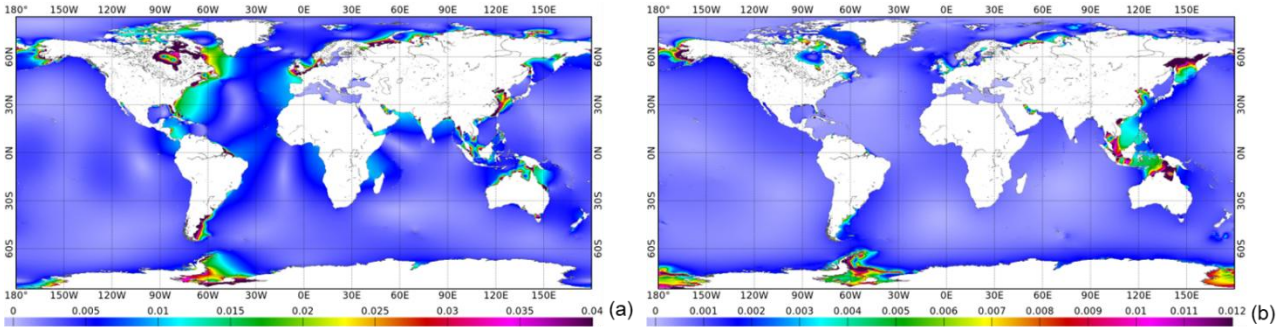


Figure 6: Root mean square (in meters) of the M2 (a) and K1 (b) amplitude variations from the ensemble of simulations.

4.2 Selection of assimilated data

The data selection for the assimilation was made progressively, starting with altimetry observations and then in situ data, adding the datasets one by one. This stepwise approach aimed to assess the individual impact of each dataset, and maintain a sober approach, preventing overfitting of the hydrodynamic model in regions where errors are minimal.

The construction of the assimilated dataset was mainly based on the results obtained on the tidal components M2 and K1, but the final solution was validated for each tidal component, ensuring that the assimilation process did not degrade the atlas in any region. Altimetry datasets were systematically decimated using the parameters specified in Table 10. Additional altimetry points were then strategically added to the initial dataset in regions that required more constraint. Figure 7 (a, b, c, d and e) illustrate the locations of the selected altimetry points for each dataset. A selection of 295 tide gauge observations was added (Figure 7, e). These observations were carefully selected in order to avoid overfitting the solution with very local tide features that may be inconsistent with the larger-scale tidal patterns. The full list of tide gauge stations assimilated in FES2022 is provided in the tidal atlas handbook (https://www.aviso.altimetry.fr/fileadmin/documents/data/tools/hdbk_FES2022.pdf) available on the AVISO+ website.

In the end, the FES2022 assimilated solution has been constrained for 16 tidal components, namely M2, S2, K1, O1, P1, Q1, Nu2, Mu2, N2, K2, E2, L2, La2, M4, 2N2 and J1. However, these tidal components are not all available at all assimilated points, as the analysed spectrum depends on the dataset as presented in Sect. 2.

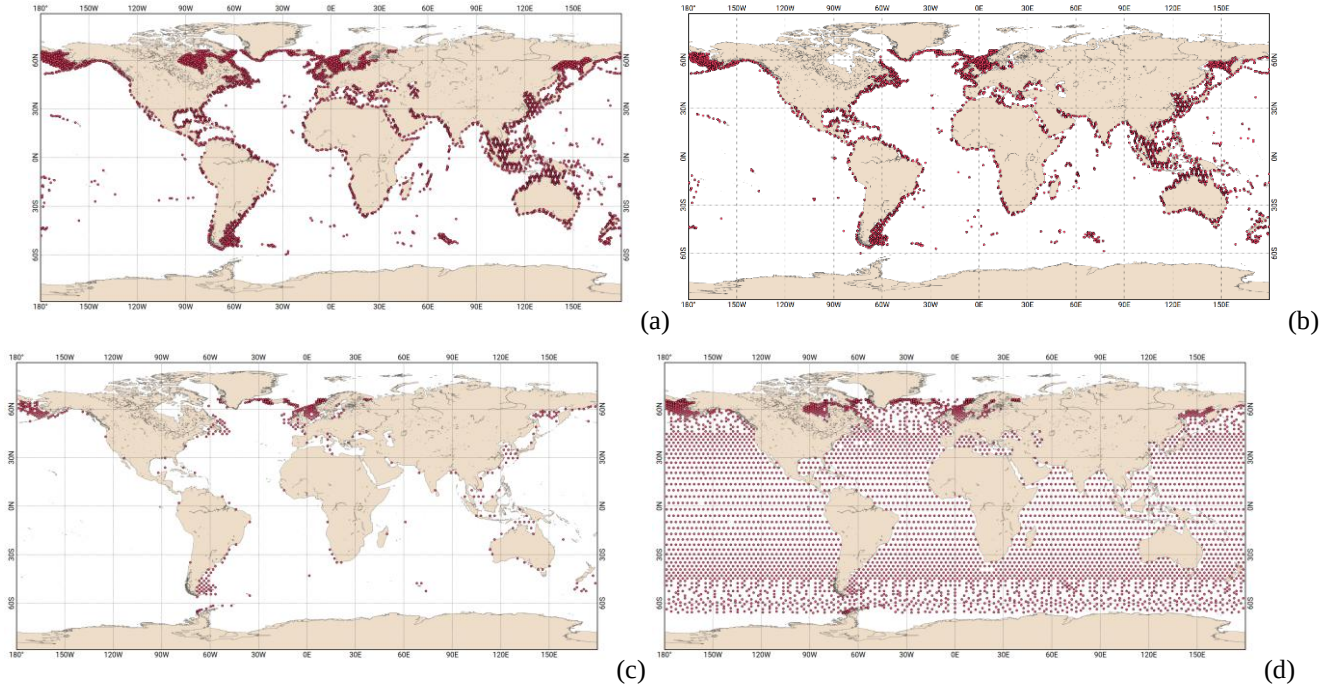
Finally, as explained in Sect. 2, the data assimilation was done twice, to take into account the loading tide deduced from the FES2022a ocean tide atlas in the altimetry dataset and thus improve the consistency between the observations and the model. Exactly the same points were assimilated to produce the final FES2022b assimilated tidal atlas.

In addition to the tidal elevations, the same data assimilation process has been applied to the tidal currents.

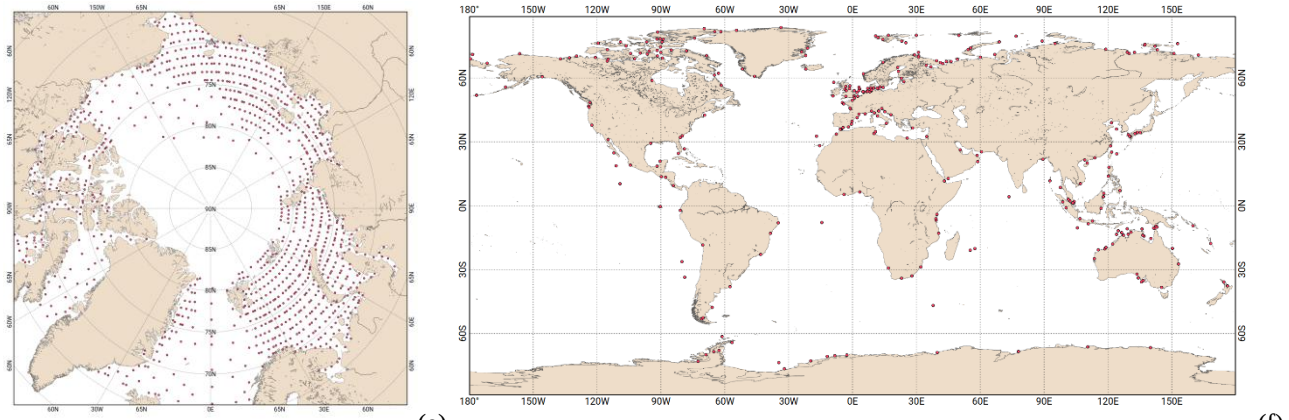
https://doi.org/10.5194/egusphere-2026-6805
Preprint. Discussion started: 11 November 2026
© Author(s) 2026. CC BY 4.0 License.

Table 10: Selection criteria of the altimetry observations for the data assimilation process and number of selected observations, depending on the mission. Deep/shelf limit indicates the 500 m isobath.

Dataset	Area	Spatial resolution for decimation	Number of observations for M2
Crossovers TPJ1J2J3	Deep Shelves	200 km 0 km	3 838 832
Crossovers TPNJ1NJ2N	Shelves	0 km	472
Along-track TPJ1J2J3	Shelves; lat > -60°N	50 km	4 069
Along-track TPNJ1NJ2N	Shelves; lat > -60°N	50km	3 270
High Latitudes (North)	Deep	200 km	82
	Shelves	50 km	926



https://doi.org/10.5194/egusphere-2026-6805
Preprint. Discussion started: 11 November 2026
© Author(s) 2026. CC BY 4.0 License.



(e) (f)

Figure 7: (a, b, c, d, e) Altimetry data selected for the data assimilation: TP-J1-J2-J3 along-track (a), TPN-J1N-J2N along-track (b), TPN-J1N-J2N crossovers (c), TP-J1-J2-J3 crossovers (d), high latitude altimetry dataset in the Arctic Ocean (e). (f) Tide gauge data selected for the data assimilation.

5 FES2022 tidal atlas assessment and validation

The FES2022b atlas is composed of 16 tidal components that benefited from the data assimilation process as described in the previous section (M2, S2, K1, O1, P1, Q1, Nu2, Mu2, N2, K2, E2, L2, La2, M4, 2N2 and J1). In addition, the spectrum has been enhanced with 18 tidal waves (M3, M6, M8, Mf, MKS2, Mm, MN4, MS4, MSf, MSqm, Mtm, N4, R2, S1, S4, Sa, Ssa, and T2) analysed from the time-stepping hydrodynamic simulations described in Sect. 3. The complete FES2022b atlas thus contains 34 tidal components.

As described in Sect. 3, the FES2022b atlas has been elaborated on a Non-Structured (NS) grid. However, to ease the use of the model for different users and applications, we provide it on a regular cartesian grid with a 1/30° resolution, which allows keeping the NS grid refinement in most coastal areas. Moreover, as the model may not be defined in all very coastal regions, due to imperfections in the coastline and bathymetry datasets, an extrapolation procedure has been applied to the tidal elevation cartesian grids. This simple extrapolation is done on 20 pixels to cover estuaries and fjords as far as possible. A mask is then applied to set all lakes and enclosed seas regions to zero. This extrapolation allows avoiding missing data due to an undefined tidal correction, but it is not perfect. Extrapolated data are flagged with a specific flag in the tidal atlas files.

This section presents the main results of the extensive validation, both in the frequency and in the temporal domains, that has been performed on the FES2022b tidal elevations and currents.

5.1 Validation of tidal elevation atlases

5.1.1 Validation in the frequency domain

The FES2022b assimilated tidal atlas has been validated in the frequency domain (i.e., wave by wave), on its native non-structured grid, against the TP-J1-J2-J3 altimetry crossover points on the shelves (less deep than 500 m) and in the deep ocean

https://doi.org/10.5194/egusphere-2026-6805
Preprint. Discussion started: 11 November 2026
© Author(s) 2026. CC BY 4.0 License.

(deeper than 500 m), as well as against the tide gauge database. Global and regional (at ocean-basin scale) results of the FES2022b atlas have been compared to those of the FES2022 hydrodynamic solution, and to the state-of-the-art global tidal models EOT20 (Hart-Davis et al., 2021), TPXO9v5 (Egbert and Erofeeva, 2002), DTU16 (Cheng and Andersen, 2017; ftp.spacecenter.dk/pub/DTU16/OCEAN_TIDE/), and GOT4.10c (Ray, 1999). The global results are presented on Figure 8 for the main tidal waves (see Table B.1 in Appendix B for all the numbers) and demonstrate that, across all tidal waves and validation datasets, the FES2022b solution consistently outperforms the other global models. The sole exception pertains to the K2 wave, where the FES2022b score against deep crossover observations is marginally larger than for EOT20, by 0.1 mm. At global scale, FES2022b exhibits strong improvements in the RSS scores, with a reduction of 0.8 mm at deep crossovers, a significant decrease of 16.3 mm (i.e., divided by almost 3) at shelf crossovers, and a substantial decrease of 51.1 mm (i.e., divided by more than 2) at tide gauges, compared to FES2014b. This underscores the substantial advancements brought by FES2022b in coastal regions, generally surpassing the most recent concurrent models, EOT20 and TPXO9v5. One can also note the clear reduction of vector differences on J1 in the FES2022 solutions, whatever the validation database, even before the data assimilation process (J1 was not assimilated in the FES2014b atlas). All these improvements can be attributed to enhancements in the bathymetry construction, the mesh resolution, and the judicious selection of assimilated observations in these regions.

https://doi.org/10.5194/egusphere-2026-6805
Preprint. Discussion started: 11 November 2026
© Author(s) 2026. CC BY 4.0 License.

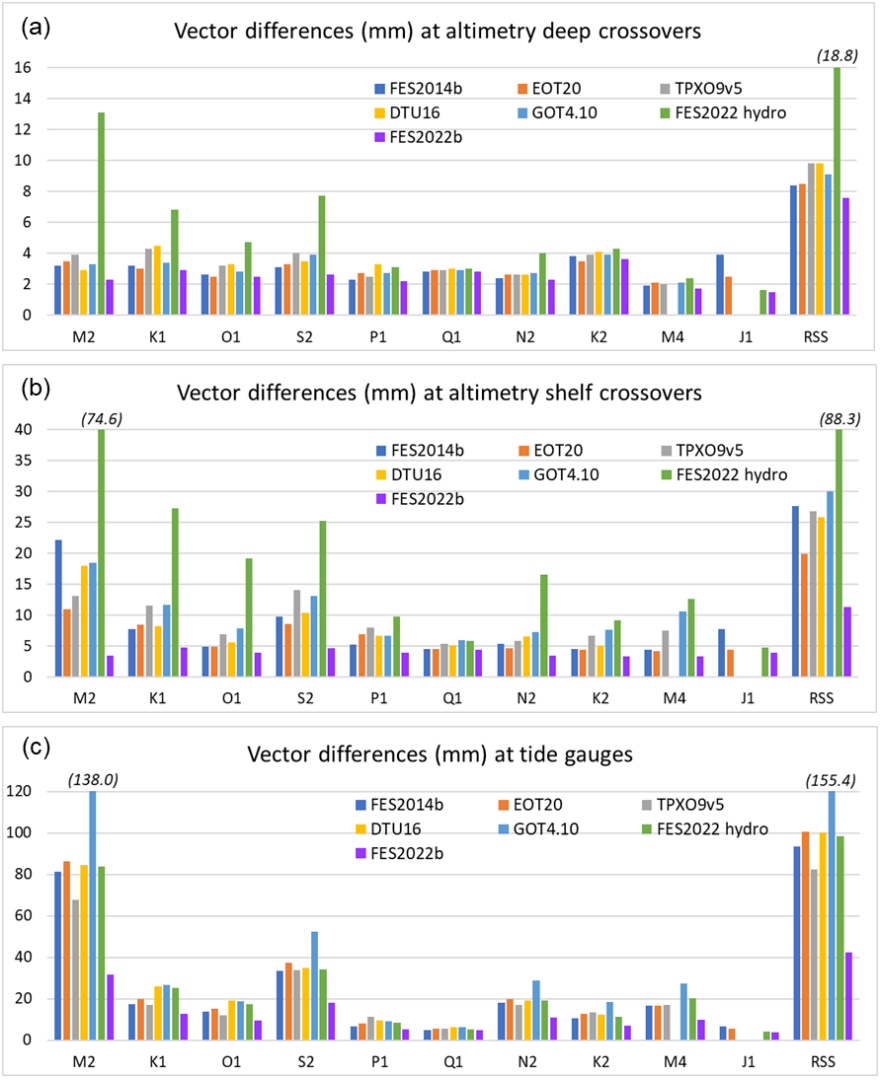


Figure 8: Global validation of the main assimilated tidal constituents (and J1): vector difference (mm) of the FES2022b solution and the other global models, against the deep crossover (a), shelf crossover (b) and tide gauge (c) validation datasets. The Root Sum Square (RSS) score is computed over the 8 main components (M2, K1, O1, S2, P1, Q1, N2, and K2). The numbers in brackets correspond to the actual values of the corresponding bars as they exceed the vertical axes.

Figure 9 shows the vector differences of the FES2014b and FES2022b M2 tidal waves at the TP-J1-J2-J3 altimetry crossover points on the shelves (for K1, see Figure B.1 in Appendix B). The differences are strongly reduced worldwide with the new FES2022b solution, which confirms the global numbers of Figure 8. Major improvements can be particularly noticed in the North East Atlantic Ocean, in the Hudson Bay, on the Patagonian Shelf, in the Yellow Sea, in the Okhotsk Sea and in the Bering Strait. A few regions still show locally large differences between the FES2022b solution and the altimetry points (e.g., around Australia and Indonesia, in the White Sea).

https://doi.org/10.5194/egusphere-2026-6805
Preprint. Discussion started: 11 November 2026
© Author(s) 2026. CC BY 4.0 License.

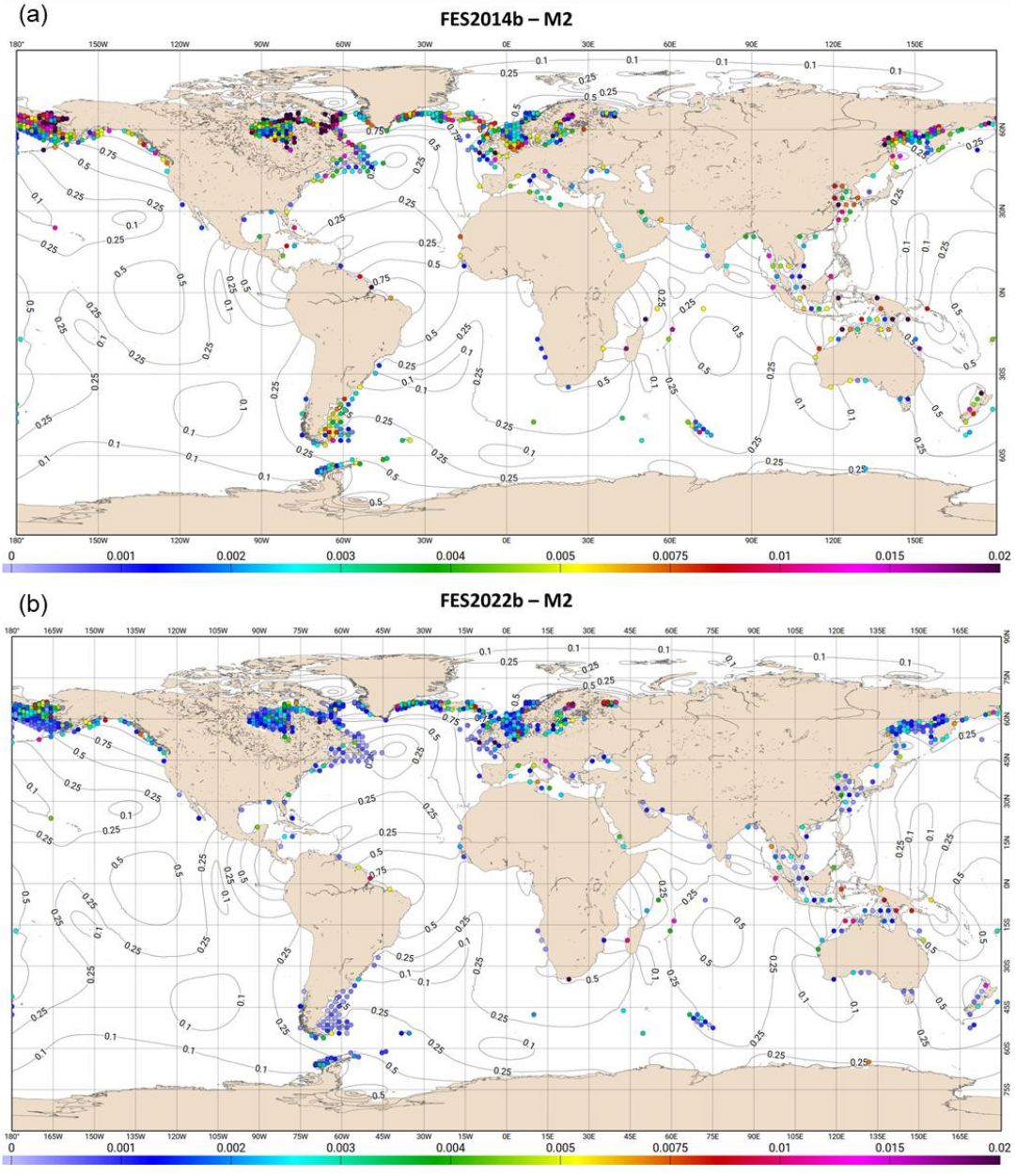


Figure 9: Vector difference (m) in color between the shelf altimetry crossover database and the FES2014b (a) and FES2022b (b) assimilated models for the M2 tidal wave. The black isolines show the M2 tide amplitude iso-contours from the models in meters.

https://doi.org/10.5194/egusphere-2026-6805
Preprint. Discussion started: 11 November 2026
© Author(s) 2026. CC BY 4.0 License.

5.1.2 Variance reduction in sea level observations

A complementary validation consists in estimating the variance reduction in altimetry and tide gauge sea level estimates obtained when applying the new FES2022b tidal model instead of other global tidal atlases to correct for the barotropic tide variability. This temporal approach allows evaluating both the modelling error of the tidal atlas and the omission error due to the missing tidal constituents in the prediction. The geocentric tide (i.e., the sum of the ocean tide and the loading tide) is used to correct the altimeter data. Only the oceanic tide is used to correct the tide gauge data as gauges are fixed to the ground and follow the tidally induced ground motion. In this section, the validation has been done with the extrapolated version of the atlas on the cartesian grid, as it is the most used by all users.

The global impact of the FES2022b tidal correction is estimated by computing the altimeter SSH differences between ascending and descending tracks at mission crossovers, using either the new tidal model or a reference one. Crossover points with time lags shorter than 10 days within one cycle are selected in order to minimize the contribution of the ocean variability at each crossover location. This diagnostic allows an accurate estimation of the impact of the tide correction on the high-frequency part of the altimeter SSH. The temporal variance of the SSH differences is computed in boxes of $4^\circ \times 4^\circ$. The analysis has been performed for several altimetry missions, but we only present here major results for Jason-3, AltiKa and Sentinel-3A. Jason-3 was the reference mission at the time of this work, and it is a very accurate mission. AltiKa and Sentinel-3A data are nearly independent of all the tested models in the global ocean as they are generally not used to constrain them through either data assimilation or optimal interpolation. Moreover, the Sentinel-3A validation period used (used 2021) is totally independent from the data assimilated into the FES2022b model.

Figure 10 shows the maps of SSH variance differences when comparing FES2022b with the FES2014b and GOT4v10c tidal models. Results demonstrate the very good performance of the FES2022b tidal solution compared to the other models: a strong variance reduction is noted in all shallow-water regions (more than 10 cm^2 when comparing to GOT4v10c and several cm^2 when comparing to FES2014b), and a reduction is also visible in some deep ocean areas. Statistics for the AltiKa mission give consistent results with those of Jason-3 on the global ocean, and they give complementary information for the high latitudes: the FES2022b model reduces significantly the altimeter SSH variance in the Arctic Ocean and in the northern parts of the Ross and Weddell seas (Southern Ocean), by several cm^2 and locally more than 10 cm^2. A few yellow/red points are visible on the AltiKa maps indicating a local variance raise, mostly likely due to some noise due to a lack of data measurements in the boxes (near sea-ice and coasts) but possibly indicating a very local degradation of the new solution. The mean global SSH variance reduction compared to FES2014b reaches 2.26 cm^2 for Jason-3 and 5.75 cm^2 for AltiKa, and is two to three times greater when comparing to GOT4v10c (5.07 cm^2 for Jason-3 and 16.6 cm^2 for AltiKa).

https://doi.org/10.5194/egusphere-2026-6805
Preprint. Discussion started: 11 November 2026
© Author(s) 2026. CC BY 4.0 License.

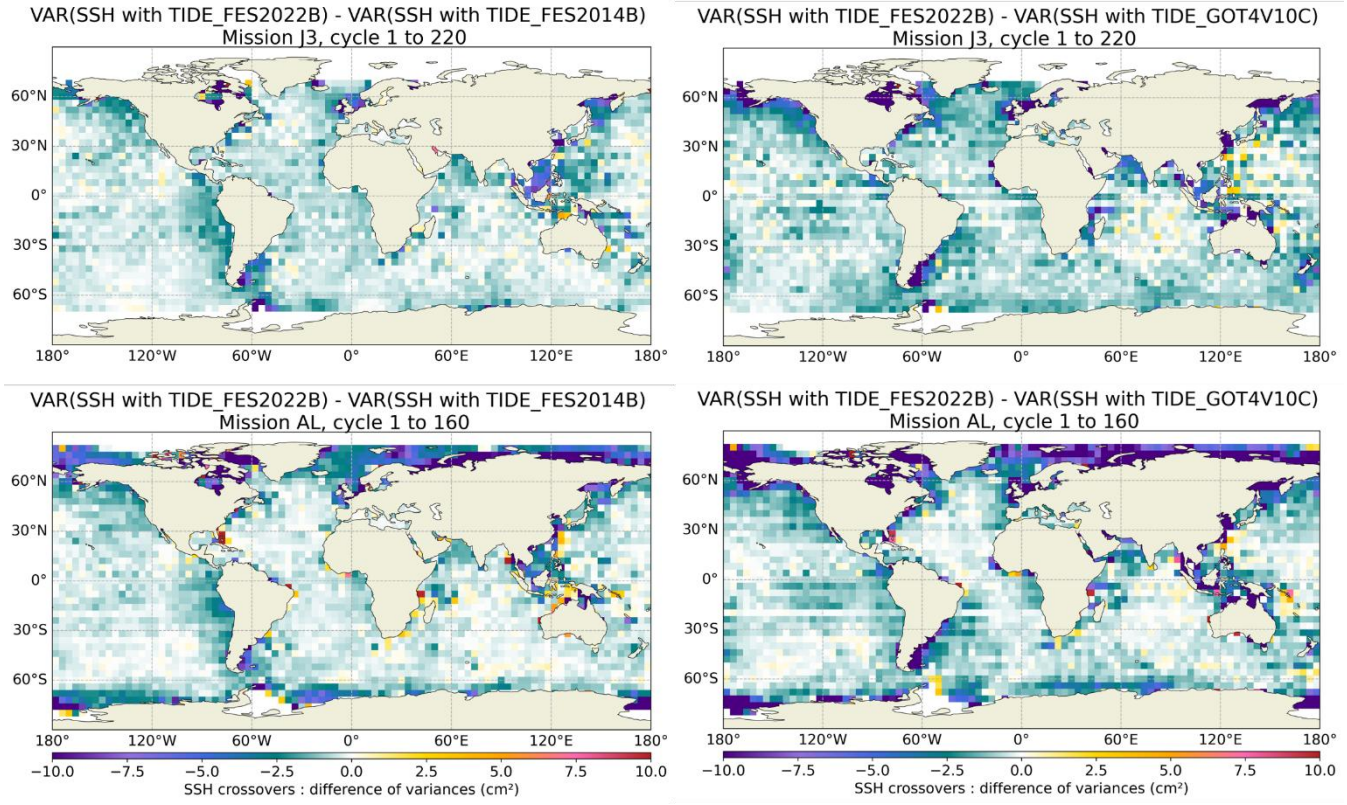


Figure 10 : Maps of SSH variance differences (in cm²) at crossovers using either the FES2022b tidal atlas or the reference tidal atlas in the SSH calculation for the Jason-3 mission (upper panels, J3 cycles 1–220) and for AltiKa (lower panels, AL cycles 1–160). The reference atlas is either FES2014b (left) or GOT4V10 (right). Greenish to blueish colors indicate a variance reduction when using FES2022b tidal correction. Tidal corrections were computed for all models with their native constituent spectrum (i.e., not restricted to common constituents).

These results in the polar seas are confirmed when looking at the SSH variance reduction using the Sentinel-3A mission over an independent period (Figure 11). Using FES2022b significantly reduces the Sentinel-3A crossover SSH variance, compared to FES2014b and GOT4v10c. The improvement occurs in all Antarctic seas. In the Arctic Ocean, it is mostly located in the Baffin Bay and on the Siberian shelf when compared to FES2014b, and in most of the Arctic areas when compared to GOT4v10c.

https://doi.org/10.5194/egusphere-2026-6805
Preprint. Discussion started: 11 November 2026
© Author(s) 2026. CC BY 4.0 License.

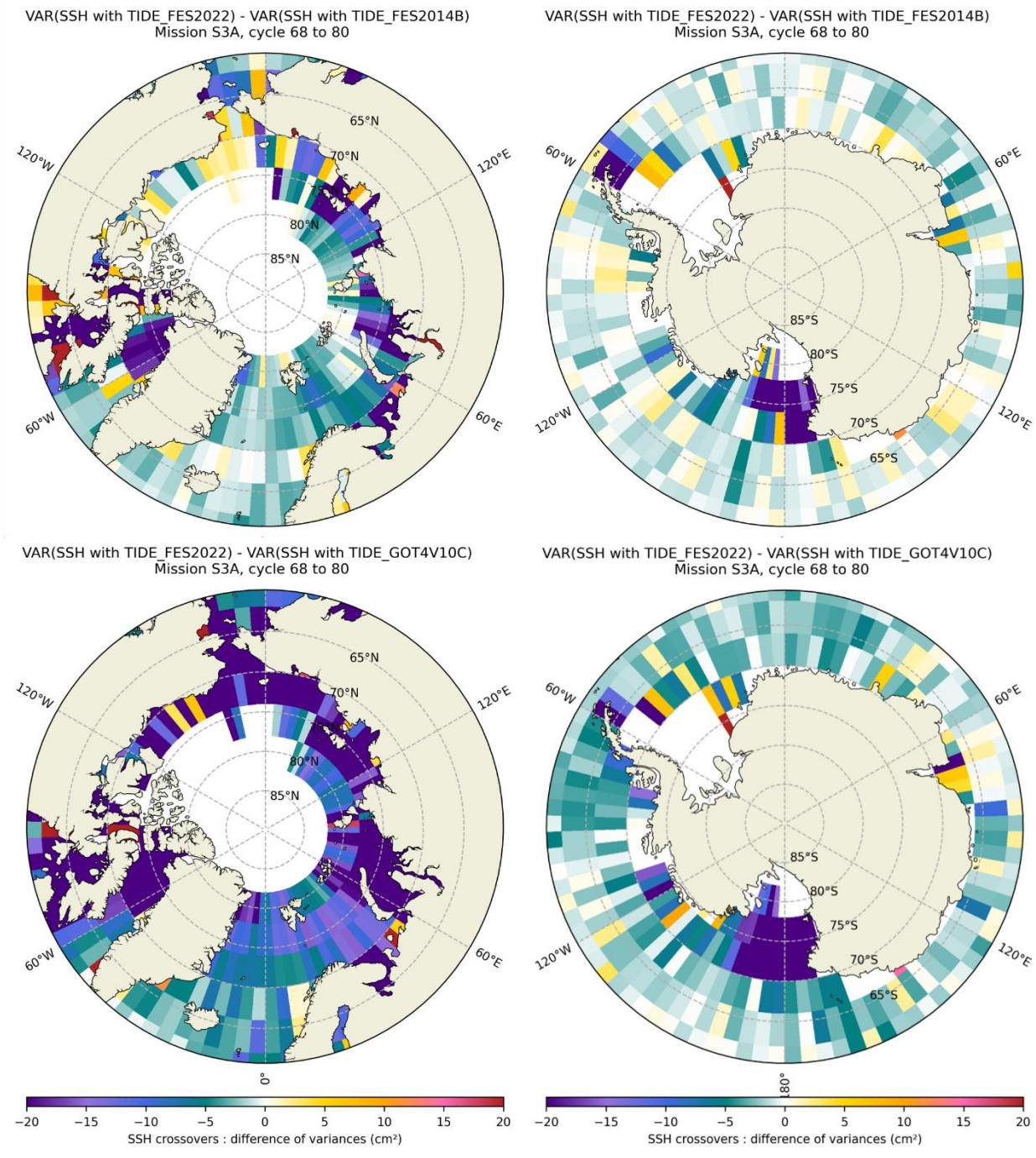


Figure 11 : Maps of SSH variance differences at crossovers in polar seas (Arctic on the left and Antarctic on the right), using either the FES2022b tidal atlas or the reference tidal atlas in the Sentinel-3A SSH calculation (one year of data: 2021). The reference atlas is either FES2014b (upper panels) or GOT4V10 (lower panels). Blueish colors indicate a higher variance reduction

https://doi.org/10.5194/egusphere-2026-6805
Preprint. Discussion started: 11 November 2026
© Author(s) 2026. CC BY 4.0 License.

when using FES2022b tidal correction. Tidal corrections were computed for all models with their native constituent spectrum (i.e., not restricted to common constituents).

The new FES2022b tidal atlas benefits from several major improvements in coastal and shallow water regions, as described in previous sections. Figure 12 shows the mean variance reduction of Jason-3 and AltiKa SLA as a function of the distance to the coast when using the new FES2022b tidal correction instead of either FES2014b or GOT4v10c. FES2022b allows a significant and increasing variance reduction when getting closer to the coast, particularly within 60 km from the coast: the mean reduction for Jason-3 SLA is over 40 cm² in the last 20 km compared to GOT4v10c and between 8-20 cm² compared to FES2014b. The mean variance reduction when approaching the coast is even stronger on AltiKa, due to the strong improvement of the model in the Arctic area, as shown previously.

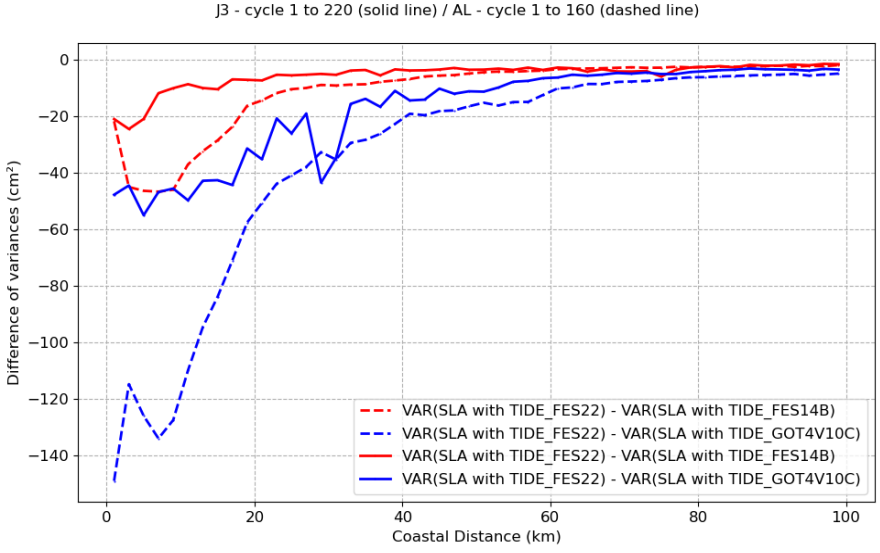


Figure 12 : Mean variance reduction of the along-track SLA (in cm²) as a function of the distance to the coast, when using the FES2022b tidal solution instead of GOT4v10c (blue lines) or FESS2014b (red lines), for the Jason-3 (solid lines) and AltiKa (dashed lines) missions.

We also compared the FES2022b tidal predictions with tide gauge time series from the GLOSS-CLIVAR database distributed by the University of Hawaii Sea Level Center (https://uhslc.soest.hawaii.edu/data/). Figure 13 shows the map of the variance reduction for each tide gauge time series when using the new solution instead of FES2014b or GOT4v10C. In both cases, dots are mostly blue, indicating a variance reduction when using FES2022b except for a few points in red and orange where the new model increases the variance. The mean global variance reduction is 9.15 cm² when using FES2022b instead of GOT4v10c, and nearly 2 cm² when comparing to FES2014b (mean statistics are computed on a selection of tide gauges with variance difference below 100 cm² to exclude unrealistic extremum).

https://doi.org/10.5194/egusphere-2026-6805
Preprint. Discussion started: 11 November 2026
© Author(s) 2026. CC BY 4.0 License.

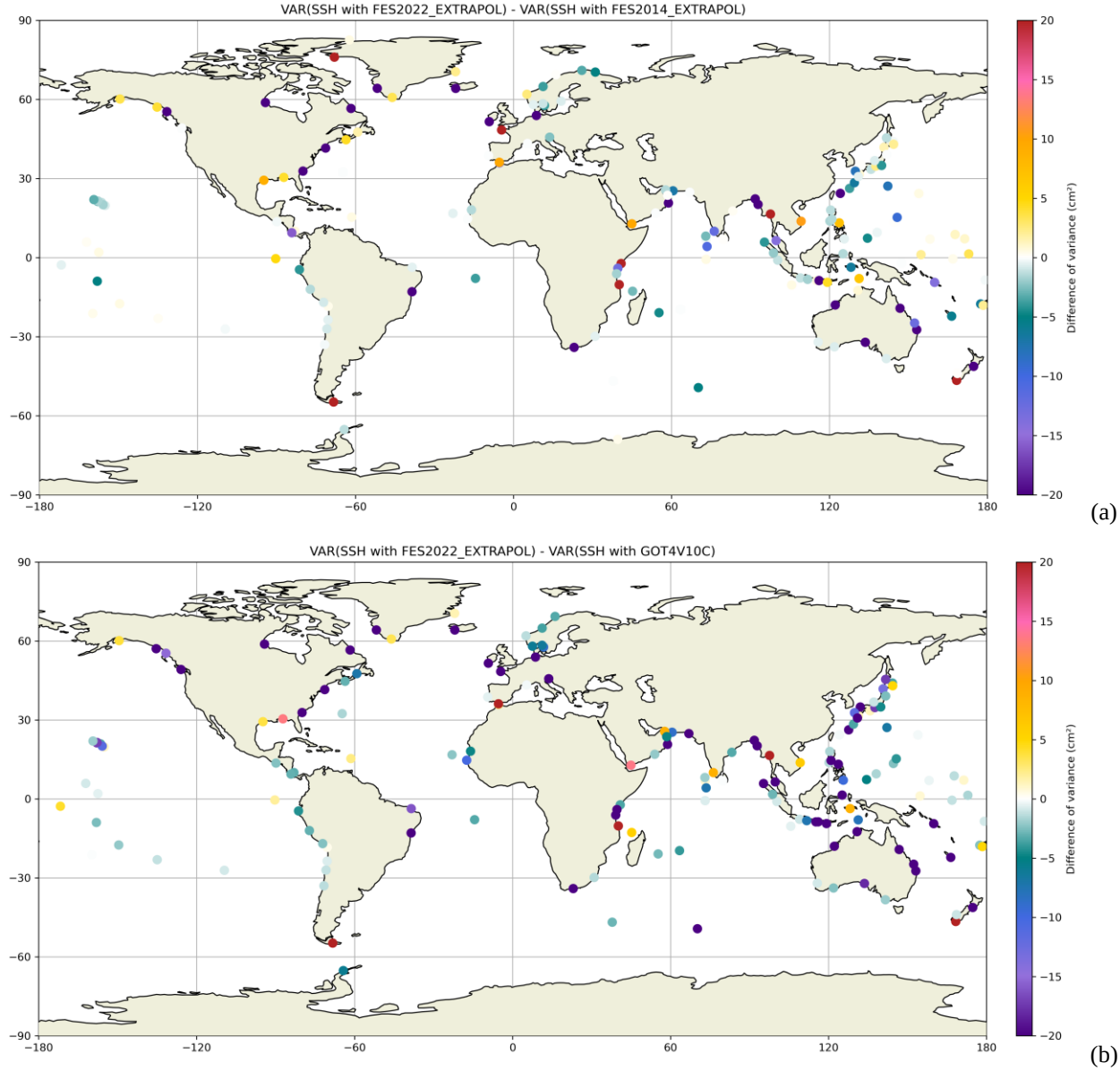


Figure 13: Maps of SSH variance differences for the GLOSS-CLIVAR tidal gauges database when using either the FES2022b tidal atlas or the reference tidal atlas in the SSH calculation (in cm²). The reference atlas is either FES2014b (a) or GOT4V10 (b). Blue color indicates a larger variance reduction when using FES2022b tidal correction

5.1.3 Reduction of GRACE gravity anomalies

An additional and novel validation method consists in computing GRACE gravity fields residual errors at tidal frequencies, considering various tidal atlases. In Figure 14, the FES2014b and FES2022b processing residuals globally show very similar

https://doi.org/10.5194/egusphere-2026-6805
Preprint. Discussion started: 11 November 2026
© Author(s) 2026. CC BY 4.0 License.

patterns. A few areas show a net improvement (i.e., lower residuals) when using FES2022b de-aliasing. This is the case for the Hudson Bay/Foxe Basin region (south of the Canadian Archipelago), but also in some smaller areas such as the Southern Great Barrier region, the Northern Australian Shelf area, and the Vancouver Island region. Among the improved regions, some are linked to the higher FES2022 mesh resolution, which allows for properly discretizing some nearly closed macro tidal bays that were not discretized in the FES2014 mesh. A striking example is the Vancouver Island region (Figure 15) where the GRACE gravity field residual errors decrease from about 10 cm to 3 cm in Equivalent Water Elevation (EWE) when using FES2022b instead of FES2014b, as the FES2022 grid covers the whole island and its resolution is much higher in the region.

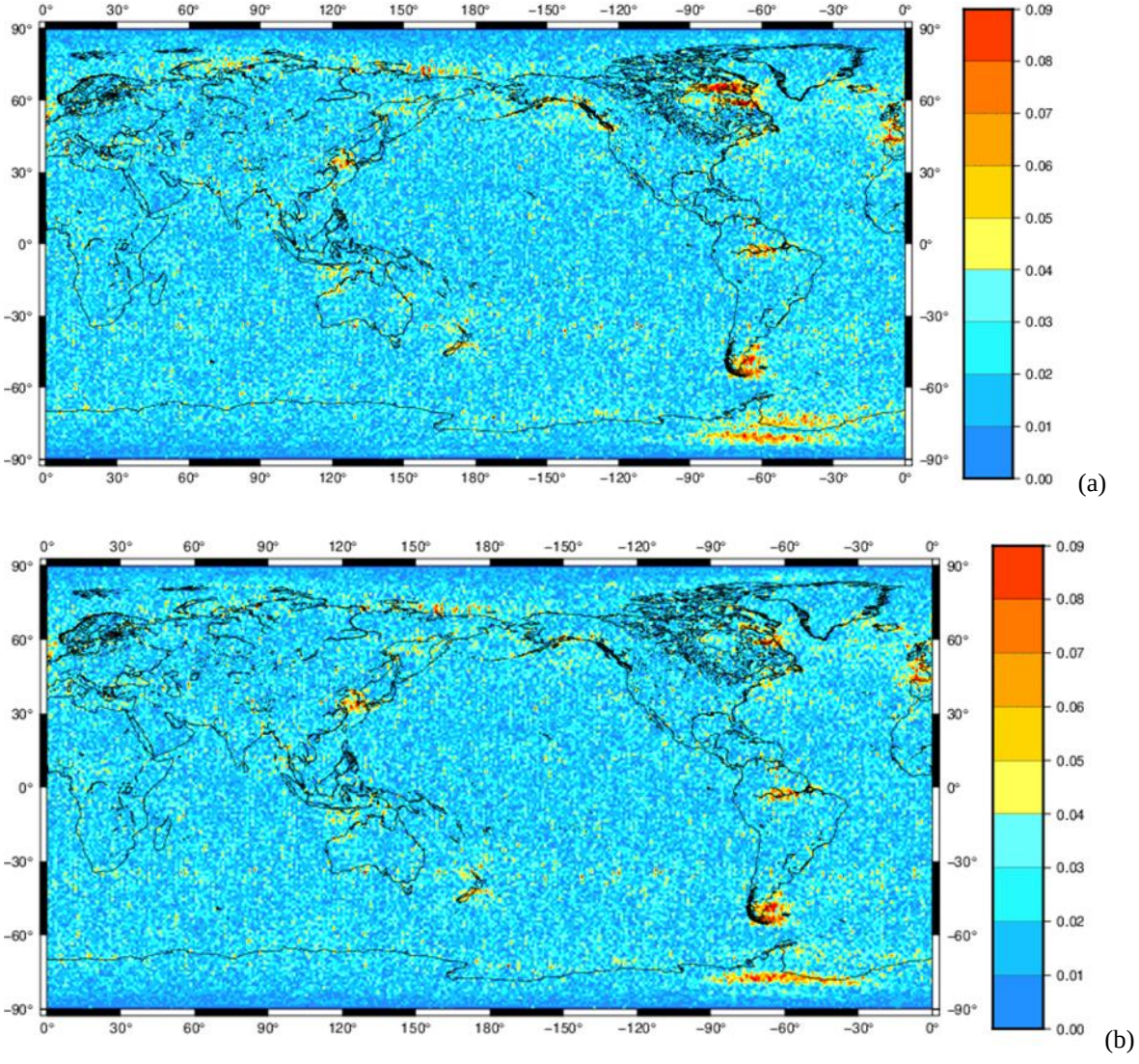


Figure 14: GRACE gravity field residuals errors at M2 frequency, by applying tidal de-aliasing from FES2014b (a) and from FES2022b (b). Units in Equivalent Water Elevation (EWE) in meters.

https://doi.org/10.5194/egusphere-2026-6805
Preprint. Discussion started: 11 November 2026
© Author(s) 2026. CC BY 4.0 License.

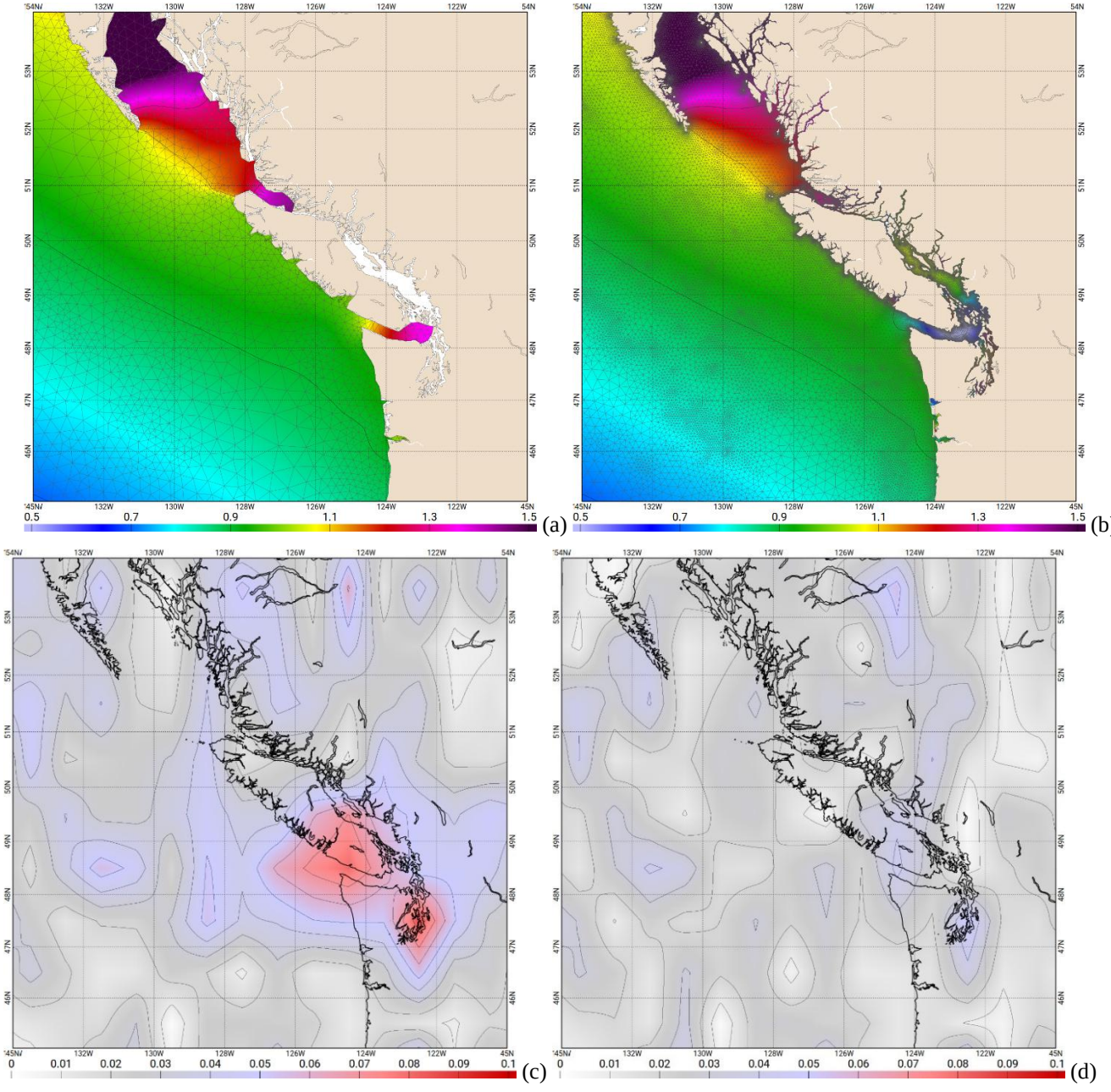


Figure 15: (a and b) Amplitude (in m) of the M2 tidal elevations in the FES2014b (a) and FES2022b (b) models, in the Vancouver Island region. The triangles of the unstructured grid of the model are superimposed on each plot. (c and d) GRACE gravity field residuals errors at M2 frequency, by applying tidal de-aliasing from FES2014b (c) and from FES2022b (d) in the Vancouver Island region. Units in Equivalent Water Elevation (EWE) in meters.

https://doi.org/10.5194/egusphere-2026-6805
Preprint. Discussion started: 11 November 2026
© Author(s) 2026. CC BY 4.0 License.

5.2 Validation of the FES2022 tidal currents

To evaluate the performance of the FES2022b tidal currents in different geographic locations around the world, a current-meter subset was carefully selected from the Global Multi Archive Current Meter Database (GMACMD, Scott and Furnival, 2013) and the Integrated Marine Observing System (IMOS, https://imos.org.au/) datasets. GMACMD contains 76 885 time series records from 1960 to 2013, either from single current meters or from moorings that provide current information at several depths. The records last from a few hours to more than 900 days, depending on the stations. The stations were selected with the following criteria: time step below 60 minutes, time series longer than 300 days, located in regions where M2 tidal current amplitude are larger than 10 cm s^{-1}. Once the criteria were applied, 73 moorings remained, with more than 85 % of these observations recorded during the 1983-2000 period. In order to expand the spatial coverage of the study, 44 Acoustic Doppler Current Profiler (ADCP) stations around Australia, provided by IMOS, were added to the dataset. Eventually, we considered 119 stations distributed in eight regions (Figure 16).

Each raw time series of the velocity components has been submitted to several diagnoses in order to assess the accuracy and consistency of the selected records. Then, the velocities at the moorings with more than one current meter were depth-averaged to obtain the barotropic component. Finally, we performed a harmonic analysis on the in situ current time series to estimate nine main tidal constituents (M2, O1, P1, K1, Q1, N2, S2, K2, M4), and we calculated the relevant tidal ellipse parameters to compare with the currents from the FES2014b, TPXO9v5 and FES2022b models.

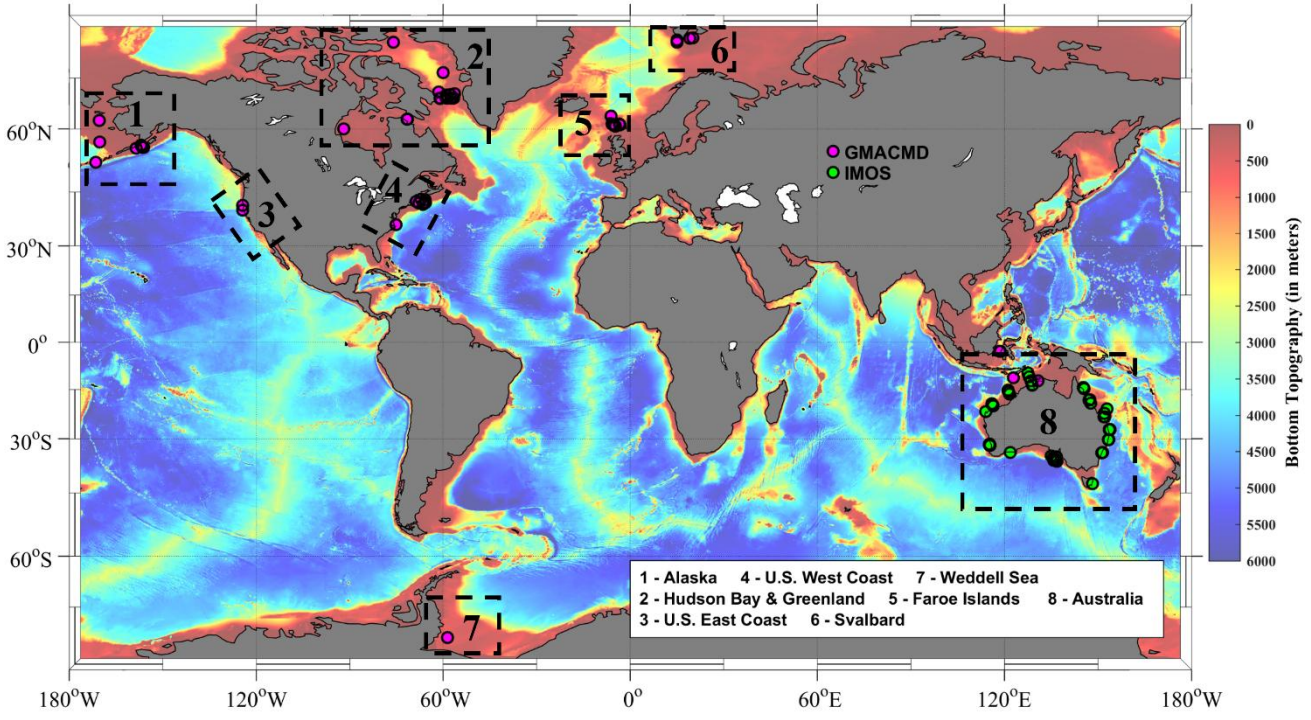


Figure 16: Locations of the selected current records, superimposed on the bottom topography (m). GMACMD and IMOS databases are respectively identified by magenta, yellow and green circles. Dashed black rectangles correspond to each area of interest.

https://doi.org/10.5194/egusphere-2026-6805
Preprint. Discussion started: 11 November 2026
© Author(s) 2026. CC BY 4.0 License.

Figure 17 shows the average Root Mean Square Differences (RMSD) between in-situ and model velocities for the major axis of the tidal ellipses in the eight selected regions and at global scale. It represents the mean bias error estimated for the main direction and amplitude of the tidal flow, between the tidal velocities of the models and the in-situ observations. An overall significant improvement in accuracy is observed with FES2022b, reducing the RMSD down to 2 cm s^{-1} for the major axis of the tidal ellipses at global scale, which represents an improvement of about 56 % relative to FES2014b and 66 % relative to TPXO9v5. Depending on the models, the largest improvements with FES2022b are obtained in Alaska, along the eastern and western coasts of the USA, and in Australia. Most of the stations evidence a significant decrease in the RMSD as a result of the better performance of FES2022b in the along bathymetry velocity component, which is mainly due to improvements of its mesh grid resolution.

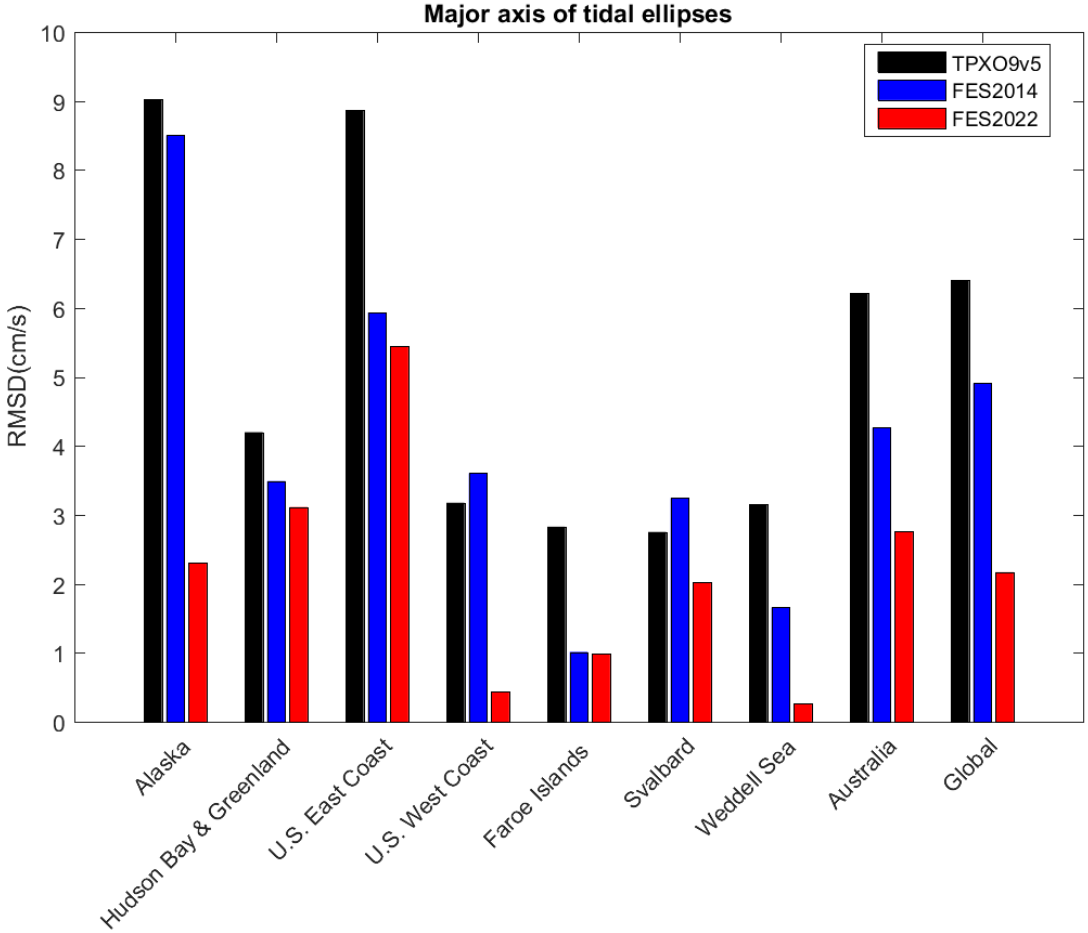


Figure 17: Average root mean square differences between in-situ and model velocities for the major axis of the tidal ellipses at global scale (right-hand bars) and in each of the eight areas. In situ vs FES2022 are indicated in red, in situ vs FES2014 in black and in situ vs TPXO9v5 in blue.

https://doi.org/10.5194/egusphere-2026-6805
Preprint. Discussion started: 11 November 2026
© Author(s) 2026. CC BY 4.0 License.

6 FES2022 Loading and Self-Attraction (LSA) atlas

The method used for the computation of the FES2022 LSA is iterative and the same as for FES2014, as described in Lyard et al. (2021) and in Sect. 2.1.1 and Sect. 3.2.1. The FES2022 LSA atlas has been computed from the FES2022b ocean tide atlas. In the pre-FES2014 era, LSA atlases were computed from the projection of the native finite element tidal elevation upon a high-resolution regular grid, either using spherical harmonics/Love numbers approach or an equivalent Green function convolution. However, T-UGOm tidal models need the gradient of LSA, obtained first through a projection back to finite element grid, then followed by a numerical derivation. The two-way projection can trigger some undesirable numerical effects, and consequently our software has been developed to directly derive the LSA atlases on the finite element grid, using Green function convolution (Lyard et al., 2021). The Love numbers have been computed by Gégout et al. (2010) using the Earth model REF_6371, and the corresponding Green functions have been derived from these Love numbers. The use of Green functions instead of Love numbers (acting on spherical harmonics decomposition of tidal complex elevation) is aimed to avoid Gibbs spurious oscillations. This is at the price of a higher computational cost, but remains a limited inconvenient when handling frequency-domain atlases.

FES2022 and FES2014 LSA atlases show limited differences in the open ocean, except in the polar seas where data assimilation control on the solutions is weaker (due to the TP/Jason inclination limited to 66° in latitude). Slightly larger differences are observed in coastal and shelf areas (see Figure 18 for the M2 tides). As one could expect, larger LSA differences occur in regions where the tidal elevation solutions show the largest discrepancies. In some places, like the Vancouver Island, the LSA differences are quite large, which is explained by the much higher resolution of FES2022 that allowed to include narrow, macro-tidal straits and channels that were omitted in FES2014, inducing an unrealistic local amplification of the tidal elevations (see Figure 15 in Sect. 5.1.3). The resulting difference in terms of tidal loading is shown on Figure 19.

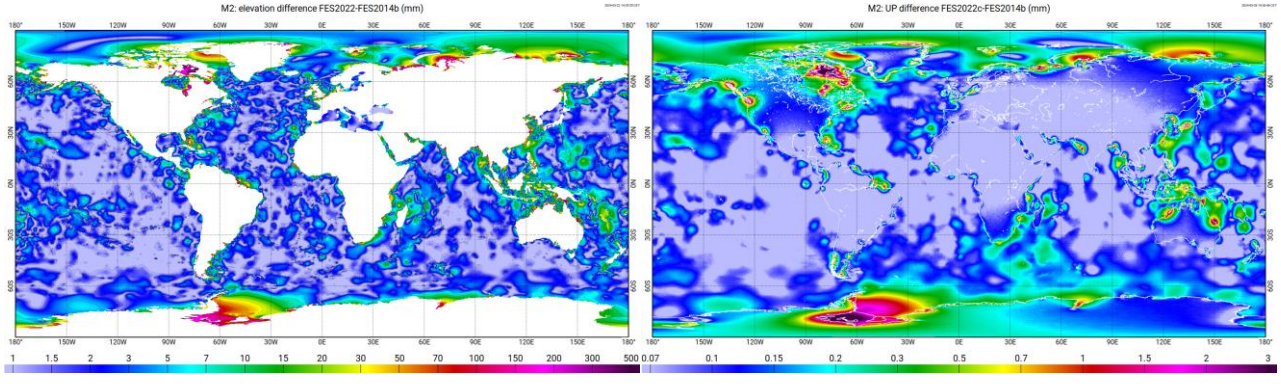


Figure 18: Vector difference (in mm) between FES2022b and FES2014b atlases for the M2 ocean tide elevations (left) and the M2 vertical loading (right).

https://doi.org/10.5194/egusphere-2026-6805
Preprint. Discussion started: 11 November 2026
© Author(s) 2026. CC BY 4.0 License.

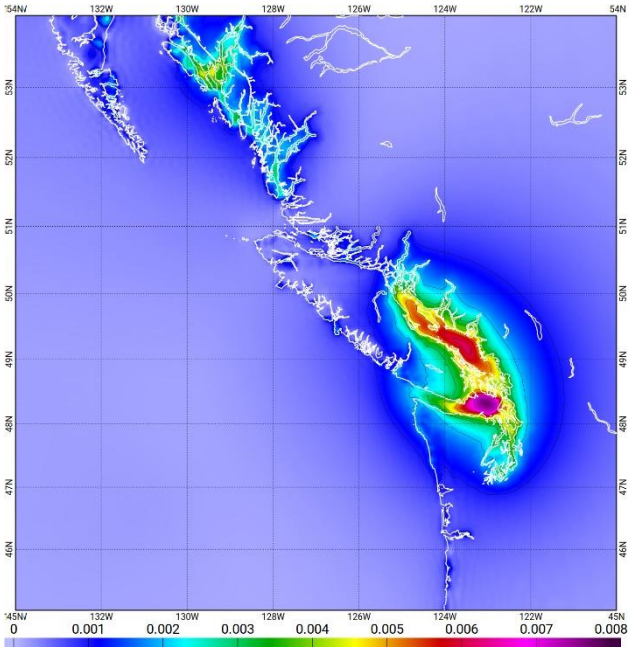


Figure 19: Vector difference (in m) between FES2022b and FES2014b for the M2 vertical loading in the Vancouver Island region.

Despite less than one centimeter, the difference is quite large (compared to the typical range of vertical displacement) and spans over an area of nearly 100 000 km². The direct validation of tidal loading vertical displacement is a quite difficult task, as the accuracy of standard GNSS-derived ground-truth data is barely adequate to conduct a meaningful atlas assessment.

7 Conclusions et perspectives

Throughout successive versions, the FES tidal atlas production team has pursued the goal of continuously improving the quality of these atlases in terms of accuracy, resolution, and coverage of the coastal zone. The FES2022 Global Tide atlas represents a major improvement in global tidal modeling, specifically designed to meet the unprecedented high-resolution demands of the SWOT mission, in particular thanks to its unstructured mesh designed to prioritize coastal and shelf regions to better capture fine tidal scales. Building upon the robust foundation of its predecessor, FES2014, this new atlas addresses critical gaps in coastal, shelf, and polar regions where earlier models exhibited significantly lower performance.

With a tenfold increase in mesh resolution, FES2022 aligns with the KaRIn instrument's 2km/500 m resolution capability, making it the first global tidal model near-compliant with SWOT's requirements in terms of tidal corrections' resolution. More generally, FES2022 atlas improvements have been carried out to narrow the gap between the resolution of modern altimetry observations (SAR, interferometric) and the resolution of the tidal atlases from which de-aliasing corrections are processed. The integration of GEBCO_2020 as the primary bathymetric dataset, supplemented by regional patches, ensures a more accurate representation of shallow-water and polar tides. The T-UGOm hydrodynamic configuration has been carefully and

https://doi.org/10.5194/egusphere-2026-6805
Preprint. Discussion started: 11 November 2026
© Author(s) 2026. CC BY 4.0 License.

regionally calibrated in order to obtain the best possible simulation, and to minimize the weight of data assimilation in the final tidal atlas.

Like for the FES2014 tidal atlas, data assimilation in FES2022 employs an ensemble Kalman filter with more than 350 members, generated by perturbing regionally the bathymetry, and the bottom friction and wave drag parameters. For FES2022, the bathymetry ensemble was enhanced by a perturbation of the model's minimum depth threshold. The assimilation process was conducted in two iterations to incorporate the FES2022a LSA solution, thereby improving the consistency between the model and the observations. The main assimilated dataset consists of harmonic analyses of nearly 30 years of the most up-to-date sea level anomalies from the TP/Jason satellite altimetry missions at crossover points of the nominal orbit, supplemented by CryoSat-2, ERS/Envisat/Altika, Sentinel-3, GFO, and HY2 binned data in high northern latitudes, and by TP/Jason along-track data from the nominal and interleaved orbits, as well as tide gauge data, over continental shelves. A total of 16 tidal constituents were assimilated, supplemented by 18 additional waves derived from time-stepping simulations. This comprehensive approach has led to substantial improvements in tidal elevation accuracy compared to FES2014 and other contemporary models such as GOT4.10c. Thanks to its unprecedented coastal and shelf resolution, FES2022 is much more accurate than earlier FES atlases in shallow regions, as far as the local underlying bathymetry is also accurate. In polar regions, FES2022 significantly reduces SSH variance in the Arctic (Baffin Bay, Siberian Shelf) and Antarctic (Ross and Weddell Seas), demonstrating its robustness in high-latitude environments where data coverage has historically been limited. The FES2022 LSA atlas estimated from the FES2022 ocean tide atlas shows limited differences with the FES2014 LSA atlas, except in the polar regions and in coastal and shelf seas, where the higher resolution of the FES2022 grid has locally improved the solution (like around the Vancouver Island). The increase in the grid resolution is also beneficial to the FES2022 tidal currents atlas, as shows the validation against tidal currents estimated from in situ measurements.

However, with no surprise, the FES2022 atlas is not free of defects. Continuous validation investigations have pointed out issues related to errors in the bathymetry databases, and local inaccuracies in the shoreline databases. Although tremendous progress and effort have been made this last decade, the bathymetry is still the main source of errors in the model. These errors not only impact the hydrodynamic model configuration, but also deteriorate the realism of the model error covariances when building the ensemble of simulations for data assimilation, which propagates into the innovation of data assimilation toward regions less constrained by data. To some extent, this problem has been amplified in places where bathymetry is poorly known or documented by the lowering of the minimum depth threshold used in the tidal simulations to 2 meters. As a consequence, some anomalous tidal elevations can be found in some coastal, limited areas. Unfortunately, the increase of resolution in model grids tends to worsen the consequences of inaccurate bathymetry prescription, and the FES2022 atlas makes no exception to this. In addition, the FES2022 resolution has highlighted some inaccuracy issues in the shoreline databases (GSHHG v2.3.7). Not only the coastal extent can locally be misplaced (with possible resonance distortion), but inconsistencies arise between bathymetry and model grid because of shoreline issues, such as coastal communication channels located on land (hence receiving unrelated bathymetry, i.e., minimum depth threshold). In the perspective of the next FES atlas generation, for which we anticipate to pursue our effort to increase the coastal resolution, it will be mandatory not only to identify the best bathymetry

https://doi.org/10.5194/egusphere-2026-6805
Preprint. Discussion started: 11 November 2026
© Author(s) 2026. CC BY 4.0 License.

datasets, but also to do the same for the ocean shorelines (down to estuaries and deltas details), and to further verify their consistency.

FES2022 is already operationally deployed by space agencies in the processing of several altimetry missions including SWOT, Jason-3, and Sentinel-3 (Kocha et al., 2026). Its enhanced accuracy in continental shelf zones can also benefit climate studies, particularly in vulnerable coastal regions where sea-level rise signals are critical. In summary, FES2022 represents a significant improvement in global tidal modeling. While not without its limitations, its performance—superior to all existing global models in coastal, shelf, and polar regions at the time of its production—makes it an indispensable tool for modern altimetry, climate research, and operational applications. As such, FES2022 should now replace FES2014 in scientific and operational contexts. Public access to FES2022 tidal atlas is detailed in the "data availability section".

Appendix A: Altimetry data processing

The altimetry sea level anomalies (SLA) have been built using the parameters and corrections from the DT2021 database (EU Copernicus Marine Service, 2022; Faugère et al., 2022), described in Fig. A1.

This database contained the most up-to-date altimetry corrections and parameters at that time, which enabled to process more data in complex areas such as coastal regions. In addition, the altimetry time series have been extended in time, including more recent missions such as Jason-3. In the end, more tidal estimates could be computed in coastal regions, enhancing the geographical coverage of the altimetry datasets in areas where very few points were available in the FES2014 datasets (see Fig. A2 for examples of data coverage in the Philippines archipelago (a) and in the gulf of California (b)).

Once the SLA computed as described in the main part of the paper, specific processing strategies have been applied to improve the signal-to-noise ratio in the tidal harmonic analysis, particularly for the K1 and S2 tidal components. These strategies are described below.

https://doi.org/10.5194/egusphere-2026-6805
Preprint. Discussion started: 11 November 2026
© Author(s) 2026. CC BY 4.0 License.

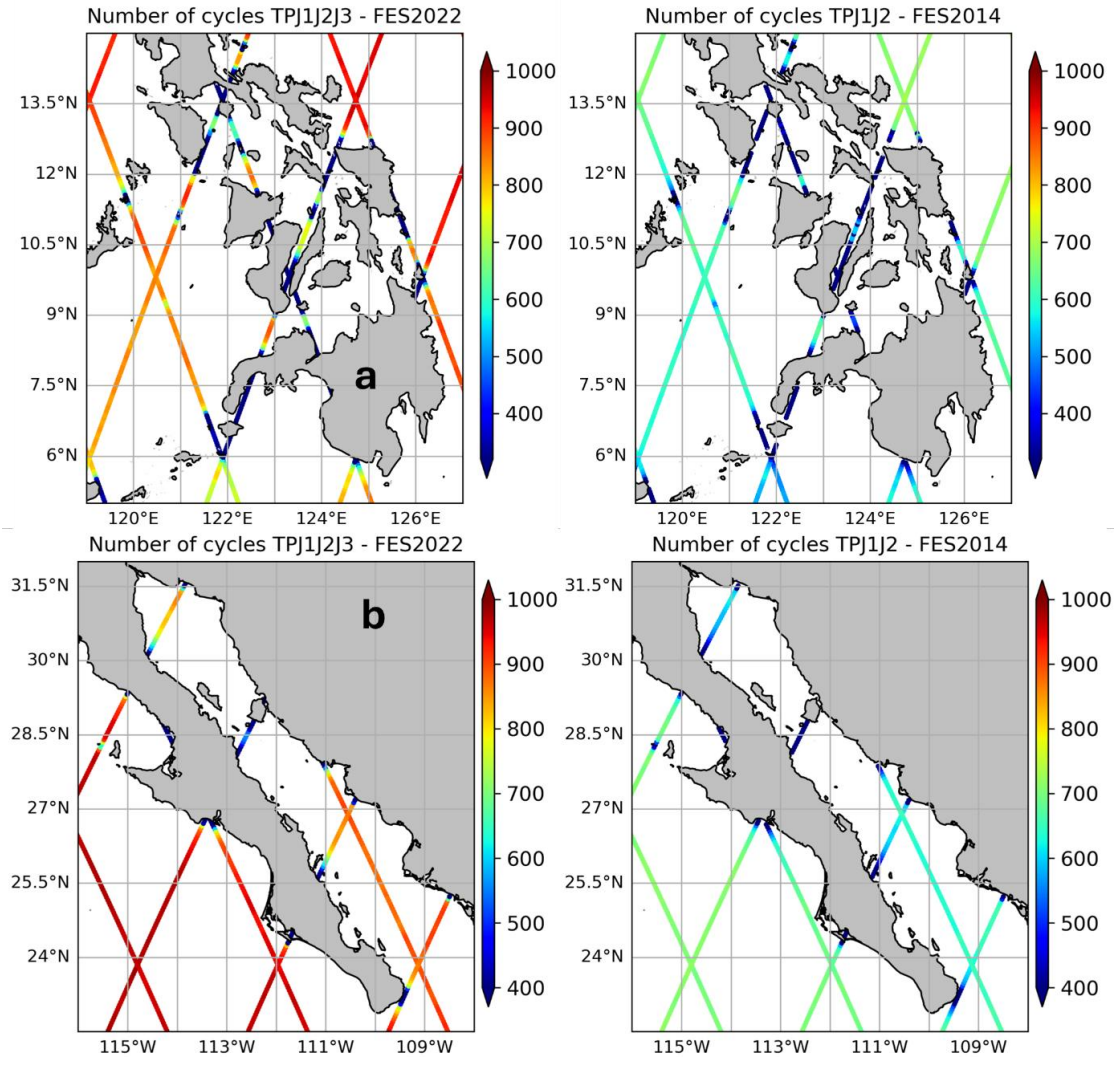
Reprocessing L2 | no update = 2018 | New for 2020

Update	Poseidon	Topex	Jason 1	Jason 2	Jason 3	ERS-1	ERS-2	ENVISAT	SARAL	Sentinel 3A	Sentinel 3B	Geosat FO	Cryosat 2	HY 2A
ORBIT	GSFC STD18		POE-E	POE-F		Reaper		POE-E	POE-F	POE-F		GSFC	POE-F	POE-D
IONOSPHERIC	DORIS	SLOOP		SLOOP (SSB C)	SLOOP	NIC09	GIM	Filtre L2 / GIM	GIM	Filtre L2		GIM		
SEA STATE BIAS	BM4	Non parametric [N. Tran 2010]	2D [N. Tran 2015]	2D J2 [N. Tran 2012]		BM3 [Gaspar Ogor 1994]	Non parametric [Mert 2005]	2D [N. Tran 2017]	2D [N. Tran 2018]	2D J2 [N. Tran 2012]		Non parametric [N. Tran & S. Labroue 2010]	2D [N. Tran 2018] Baseline C	Non Parametric [N. Tran 2012 Vent S. Labroue]
WET TROPOSPHERE	GPD+ [Fernandes et al. 2015]		JMR (GDRE) radiometer	AMR radiometer		GPD+ [Fernandes et al. 2015]		MWR radiometer reprocessed	Neuronal Network (5 entries) V4	MWR 3 radiometer		Radiometer and ECMWF	GPD+	ECMWF
DRY TROPOSPHERE	ERA5 (1-hour) model based													
DYNAMICAL ATMOSPHERIC CORRECTION	TUGO model forced with ERA 5 model				MOG2D HR forced with ECMWF	TUGO model forced with ERA 5 model			TUGO ERA 5 + MOG2D HR	MOG2D HR forced with ECMWF		TUGO forced with ERA5	TUGO ERA 5 + MOG2D HR	
OCEAN TIDE	FES 2014 B													
INTERNAL TIDE	ZARON 2019 (HRETv8.1 tidal frequencies: M2, K1, S2, O1)													
POLE TIDE	DESAI et al.2015 ; Mean Pole Location 2017													
SOLID TIDE	Elastic response													
MEAN SEA SURFACE	Composite (SCRIPPS,CNES/CLS15,DTU15)													

685

Figure A1: List of all instrumental and geophysical corrections used within the DT2021 altimeter database.

https://doi.org/10.5194/egusphere-2026-6805
Preprint. Discussion started: 11 November 2026
© Author(s) 2026. CC BY 4.0 License.



690 **Figure A2: Number of valid cycles in the FES2022 TP-J1-J2-J3 and FES2014 TP-J1-J2 along-track datasets in coastal regions, in the Philippines archipelago (a) and in the gulf of California (b).**

Correction of non-tidal signals at K1 aliased periods:

The K1 diurnal frequency is aliased close to the semi-annual frequency with the TOPEX/Jason and GFO samplings, and to the annual frequency with the ERS/Envisat/AltiKa and Sentinel-3 orbits (see Table 1 in Cancet et al., 2025). Annual and semi-
695 annual signals are quite large in the ocean dynamics, and can severely contaminate the tidal analysis. This contamination decreases with time as the square root of the record duration (Johnson and Riess, 1982), so the present very long TOPEX/Jason time-series (almost 28 years for this study) allows a very accurate estimation of all tidal components including K1. However,

https://doi.org/10.5194/egusphere-2026-6805
Preprint. Discussion started: 11 November 2026
© Author(s) 2026. CC BY 4.0 License.

the available time series are not long enough on the TPN interleaved, the ERS, the GFO and the Sentinel-3 orbits to guarantee an accurate separation of the K1 tidal signal from the semi-annual and annual ocean variability.

Previous studies (Lyard et al., 2021) showed that a preliminary correction of annual and semi-annual ocean dynamics signals allows reducing significantly the tide estimation error for the K1 frequency. For the production of the FES2014 tide model, annual/semi-annual signals were estimated from the global simulation GLORYS2v1 (Ferry et al., 2012), which does not include the ocean tide. A similar approach has been used for the production of the FES2022 altimetry database, using the most recent global model simulation GLORYS12v1 with no ocean tide (global ocean eddy-resolving reanalysis covering altimetry, E.U. Copernicus Marine Service Information (CMEMS), 2023). A harmonic analysis of the GLORYS12v1 time series has been performed on the available period (1993-2018) to extract the annual and semi-annual ocean dynamics signals (Fig. A3). These new estimations of the annual and semi-annual signals mainly show a diminution of amplitude in the Antarctic Circum-Polar area, compared to the previous estimations with GLORYS2v1. Using the GLORYS12v1 correction has a small impact on diurnal tides estimations: K1 differences between TPN-JN ascending and descending tracks are reduced by 0.1 cm (6 %) on global ocean, and differences between the estimations in high-latitude boxes and a regional tide solution in the Arctic (Cancet et al., 2018, 2022) are reduced by 45 % (0.5 cm) for K1.

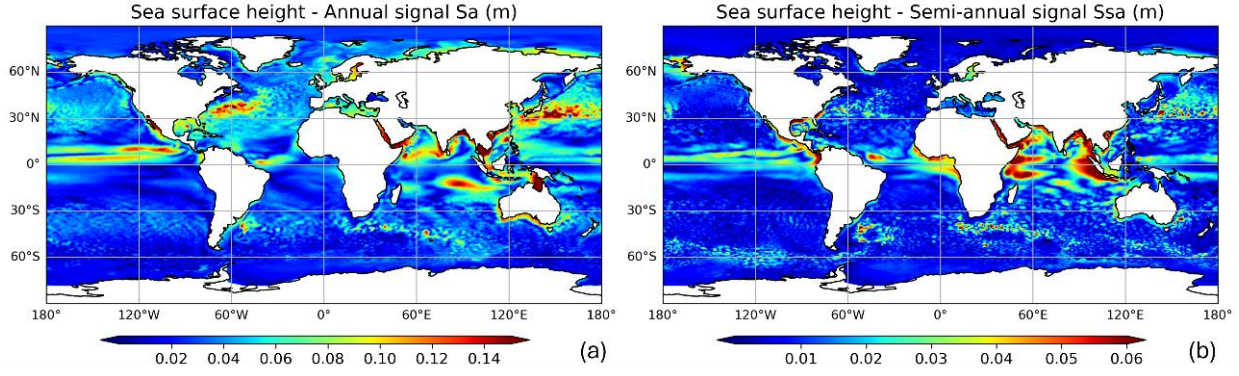


Figure A3: Estimations of the amplitude (in m) of the annual (a) and semi-annual (b) ocean dynamics signal from the GLORYS12v1 model

Filtering of internal tides surface signatures:

The model of Zaron (2019) is used to remove the coherent Internal Tide (IT) surface signal in the altimetry SLA, which is an improvement compared to FES2014, as no internal tide correction was available at that time. The SLA variance reduction on the J2 mission when using the Zaron IT correction is significant in all IT regions over the ocean (Carrere et al., 2021).

To remove the IT signal in the FES2014 altimetry dataset, a filtering approach was used (Lyard et al., 2021). Figure A4 shows the comparison of the FES2022 IT-corrected along-track altimetry M2 estimation (red) and the corresponding FES2014

https://doi.org/10.5194/egusphere-2026-6805
Preprint. Discussion started: 11 November 2026
© Author(s) 2026. CC BY 4.0 License.

altimetry M2 estimation filtered from IT (gray), along two tracks in regions where IT signals are well-known (Tahiti and Indonesian Seas). Using the Zaron IT correction allows removing most of the IT surface signature in these regions, but a small-scale signal is still visible in the FES2022 altimetry M2 estimates, that shall be filtered. An along-track spectral analysis of the tidal estimations on all the IT regions of the global ocean has been performed and points out some residual energy around the second baroclinic mode of variability (around 50-100 km) and also some noise at shorter scales (see Fig. A5 showing examples of spectra over three different regions). To remove this remaining variability, a low-frequency-pass filtering (see the wavelengths on Fig. A6) was applied using half of the wavelengths used for FES2014 (Lyard et al, 2021). Notice that FES2014 filtering wavelengths were defined upon the values of the first baroclinic wavelength and they were also constrained by the barotropic wavelength to avoid removing any barotropic signals. The FES2022 along-track filtered estimations are plotted in blue line on Fig A4, showing that most of the remaining very small-scale signatures have been cleared out.

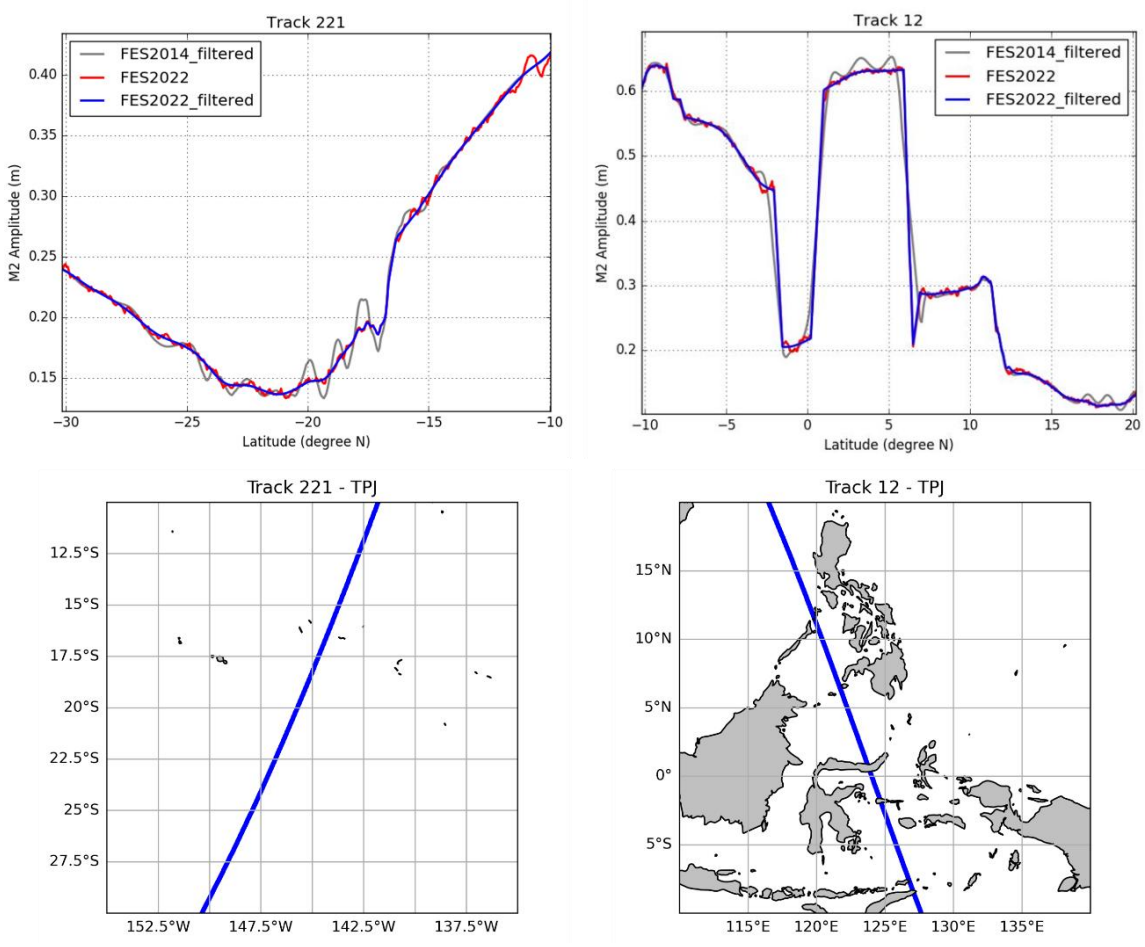
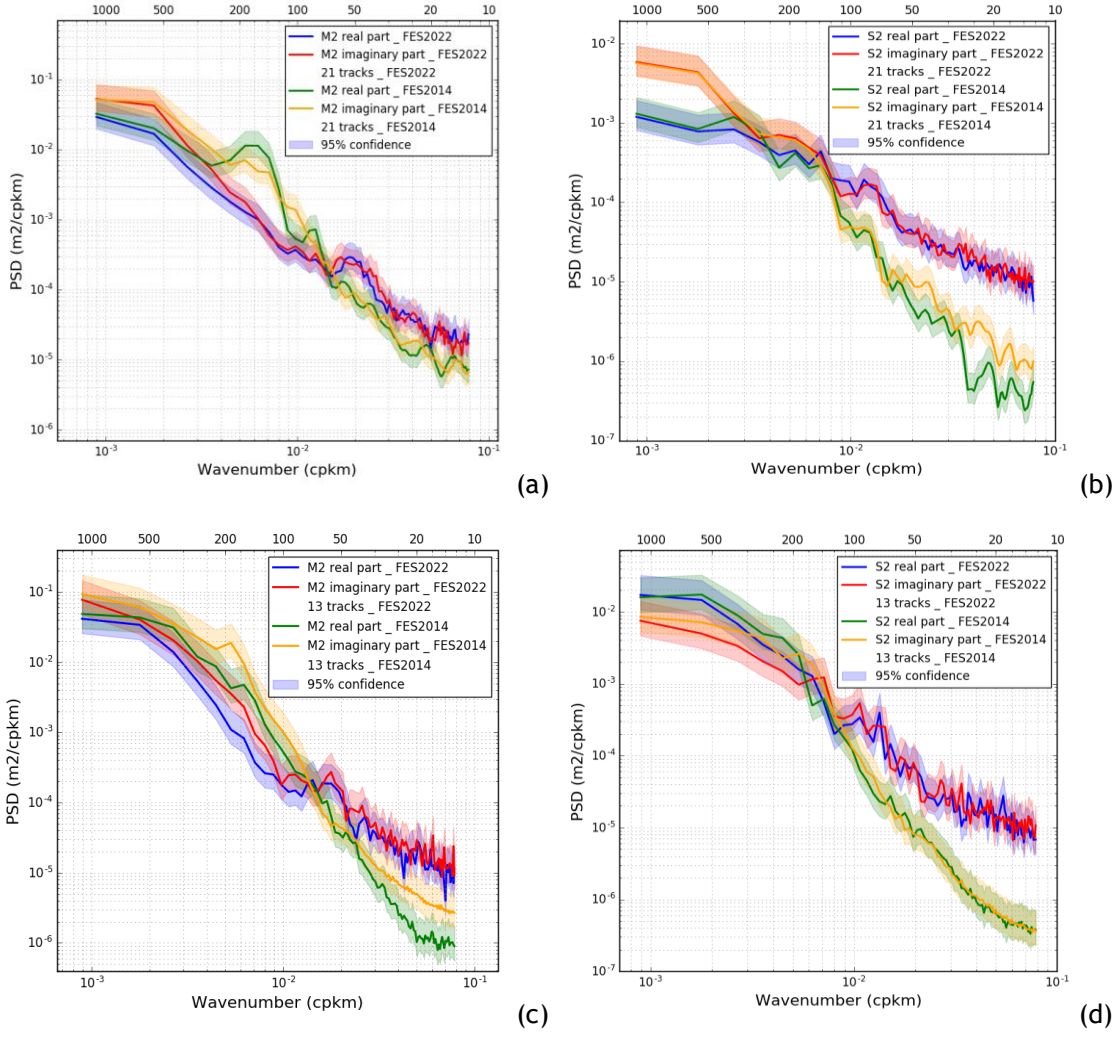


Figure A4: Comparison of FES2022 IT-corrected (red) and FES2014 IT-filtered (gray) along-track M2 estimations on TPJ tracks 221 (Tahiti) and 12 (Indonesian Seas); FES2022 IT-corrected and filtered along-track M2 estimations are plotted in blue.

https://doi.org/10.5194/egusphere-2026-6805
Preprint. Discussion started: 11 November 2026
© Author(s) 2026. CC BY 4.0 License.



https://doi.org/10.5194/egusphere-2026-6805
Preprint. Discussion started: 11 November 2026
© Author(s) 2026. CC BY 4.0 License.

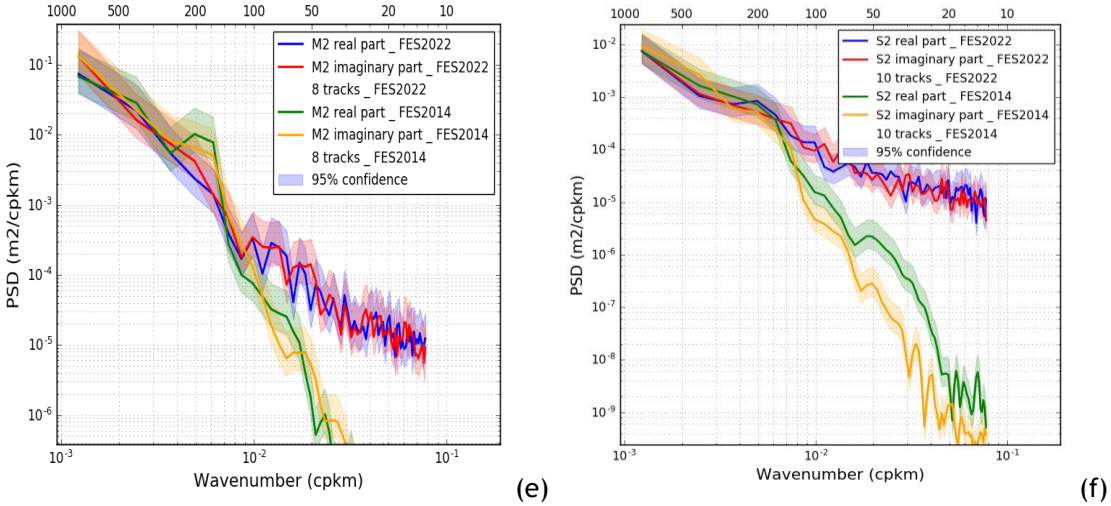


Figure A5: Along-track spectral analysis of the M2 (a, c, e) and S2 (b, d, f) estimations on the reference track TP-Jason for three IT regions of the ocean: Tahiti region (a, b), Hawaii (c, d), and the North-East Atlantic/European Shelf (e, f). FES2022 estimations are plotted in blue and red (real part and imaginary part respectively), and FES2014 estimations are plotted in green and yellow (real part and imaginary part respectively). X-axis upper scale is in km.

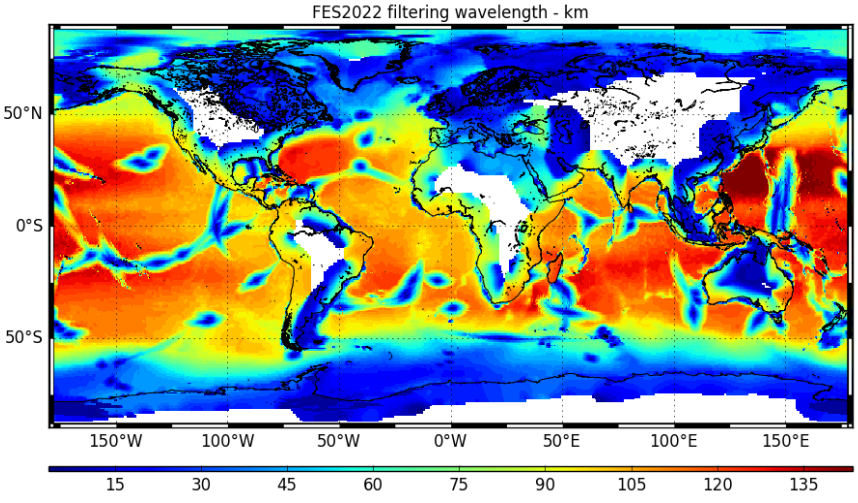


Figure A6: Map of FES2022 internal tides along-track filtering wavelengths in km.

https://doi.org/10.5194/egusphere-2026-6805
Preprint. Discussion started: 11 November 2026
© Author(s) 2026. CC BY 4.0 License.

S2 tidal constituent processing

The main semi-diurnal solar tide component S2 needs special attention because of the significant atmospheric tide forcing at this frequency. To access the pure gravitational ocean tide, in situ and satellite measurements shall be ideally corrected by the radiational tide induced by the atmospheric tide forcing, but such corrections, derived from a hydrodynamic simulation with atmospheric forcing, are not sufficiently accurate. Consequently, the choice was made to keep the entire S2 variability in the tidal estimations to fully benefit from the data assimilation step. This is an important aspect to keep in mind when combining the new FES2022 model (or any other FES tide solution as they all follow the same strategy) with a Dynamical Atmosphere Correction (surge) to compute SLAs, as it means that the S2 radiational signal must be filtered out of the surge model to avoid removing it twice.

Moreover, S2 tide is aliased to infinite period by the sun-synchronous orbits, which makes it unobservable in the ERS/Envisat/AltiKa time series, for example. With the TOPEX/Jason orbit, S2 is aliased at the 58.7-day period. Previous studies demonstrated that some residual mean sea level (MSL) signal is visible at the same frequency in the TOPEX/Jason time series, due to inaccuracy in the β prime angle that can in turn pollute tidal estimations (Zawadzki et al., 2018). However, thanks to its accurate hydrodynamic primary solution and relatively limited weight of assimilated data, the FES tidal solution is less affected by such errors than purely empirical models (Zawadzki et al., 2018).

Appendix B: FES2022 tidal atlas validation

We provide in this section complementary and more detailed validation results.

The validation scores of all the FES2022b assimilated tidal waves are presented in Table B1, considering the TP-J1-J2-J3 altimetry crossover points on the shelves (less deep than 500m) and in the deep ocean (deeper than 500m), as well as the tide gauge database. The comparison to the state-of-the-art global tidal models (EOT20, TPXO9v5, DTU16, and GOT4.10) shows the clear improvement brought by the FES2022b solution, not only on the main components, but also on secondary waves such as 2N2, L2, Mu2, Nu2, J1, E2 and La2, but also on the non-linear wave M4. Secondary tidal waves pose challenges for validation as they are difficult to accurately estimate from altimetry and tide gauge observations (unfavourable signal-to-noise ratio, time series too short for accurate separation). Caution must thus be taken for this validation, due to error estimates associated with observations that are often comparable to or larger than tidal amplitudes. Comparisons between the FES2022b and FES2014b models for secondary tidal waves generally indicate similar or better results with FES2022b.

Figure B1 shows the vector differences of the FES2014b and FES2022b K1 tidal waves at the TP-J1-J2-J3 altimetry crossover points on the shelves. The differences are globally reduced with the new FES2022b solution, and the major improvements can be noticed in the Yellow Sea, in the Hudson Bay, on the Patagonian Shelf, in the Okhotsk Sea and in the Bering Strait. A few regions still show locally large differences between the FES2022b solution and the altimetry points (e.g., in the Baltic Sea and at the entrance of the Hudson Bay).

https://doi.org/10.5194/egusphere-2026-6805
Preprint. Discussion started: 11 November 2026
© Author(s) 2026. CC BY 4.0 License.

Table B1: Global validation of all the assimilated tidal constituents: vector difference (mm) of the FES2022 assimilated (FES2022b) and hydrodynamic solutions and the other global models, against the deep altimetry crossover (upper), shelf altimetry crossover (middle) and tide gauge (bottom) validation datasets. The Root Sum Square (RSS) score is computed over the 8 main components (M2, K1, O1, S2, P1, Q1, N2, and K2) available in all the models. The bold numbers correspond to the best scores for each tidal component.

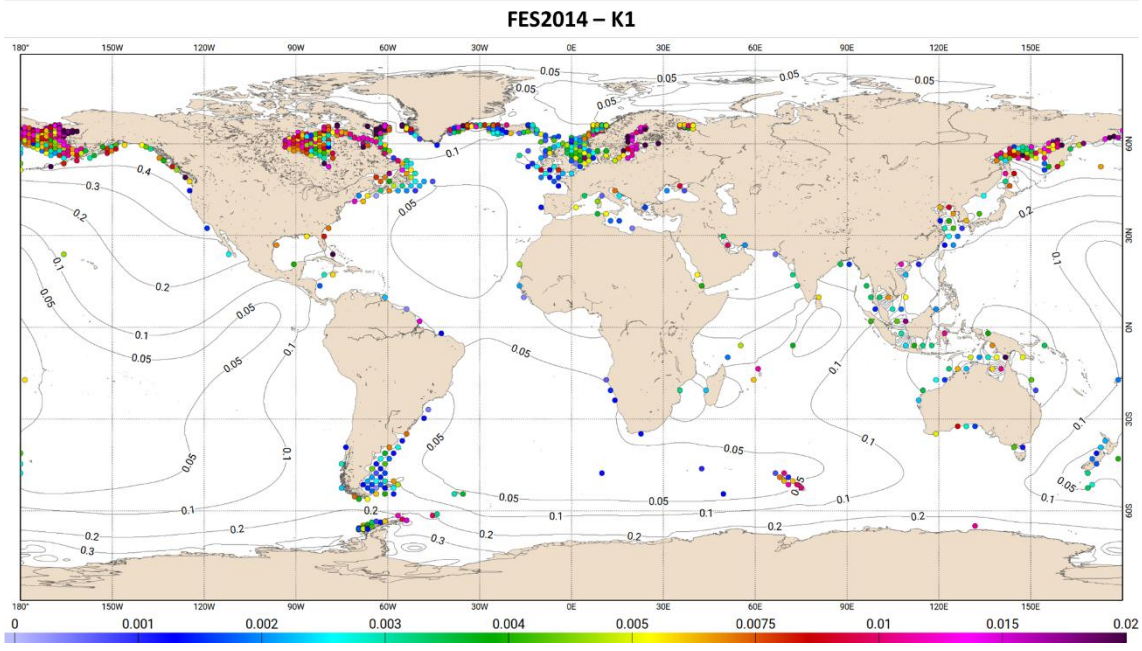
Crossover deep	M2	K1	O1	S2	P1	Q1	N2	K2	M4	2N2	L2	Mu2	Nu2	J1	E2	La2	RSS
FES2014b	3.2	3.2	2.6	3.1	2.3	2.8	2.4	3.8	1.9	1.8	1.7	1.9	2.8	3.9	2.0	1.8	8.4
EOT20	3.5	3.0	2.5	3.3	2.7	2.9	2.6	**3.5**	2.1	2.0	/	/	/	2.5	/	/	8.5
TPXO9v5	3.9	4.3	3.2	4.0	2.5	2.9	2.6	3.9	2.0	4.3	/	/	/	/	/	/	9.8
DTU16	2.9	4.5	3.3	3.5	3.3	3.0	2.6	4.1	/	/	/	/	/	/	/	/	9.8
GOT4.10	3.3	3.4	2.8	3.9	2.7	2.9	2.7	3.9	2.1	/	/	/	/	/	/	/	9.1
FES2022 hydro	13.1	6.8	4.7	7.7	3.1	3.0	4.0	4.3	2.4	1.8	2.1	3.6	2.9	1.6	1.7	2.0	18.8
FES2022b	**2.3**	**2.9**	**2.5**	**2.6**	**2.2**	**2.8**	**2.3**	**3.6**	**1.7**	**1.7**	**1.6**	**1.9**	**2.7**	**1.5**	**1.4**	**1.8**	**7.6**

Crossover shelf	M2	K1	O1	S2	P1	Q1	N2	K2	M4	2N2	L2	Mu2	Nu2	J1	E2	La2	RSS
FES2014b	22.1	7.7	4.9	9.7	5.2	4.5	5.4	4.5	4.4	3.6	4.5	6.4	4.1	7.7	6.9	4.1	27.6
EOT20	10.9	8.5	4.9	8.6	6.9	4.5	4.6	4.4	4.2	3.6	/	/	/	4.4	/	/	19.9
TPXO9v5	13.1	11.5	6.9	14.1	8.0	5.3	5.8	6.6	7.5	10.7	/	/	/	/	/	/	26.8
DTU16	18.0	8.2	5.6	10.3	6.7	5.1	6.5	5.0	/	/	/	/	/	/	/	/	25.8
GOT4.10	18.5	11.7	7.9	13.1	6.6	5.9	7.3	7.6	10.6	/	/	/	/	/	/	/	30.0
FES2022 hydro	74.6	27.3	19.2	25.2	9.8	5.8	16.6	9.1	12.6	4.3	8.9	13.9	6.6	4.8	3.8	5.9	88.3
FES2022b	**3.4**	**4.7**	**3.9**	**4.6**	**3.9**	**4.4**	**3.4**	**3.3**	**3.3**	**3.2**	**4.2**	**4.2**	**3.7**	**3.9**	**3.4**	**4.1**	**11.3**

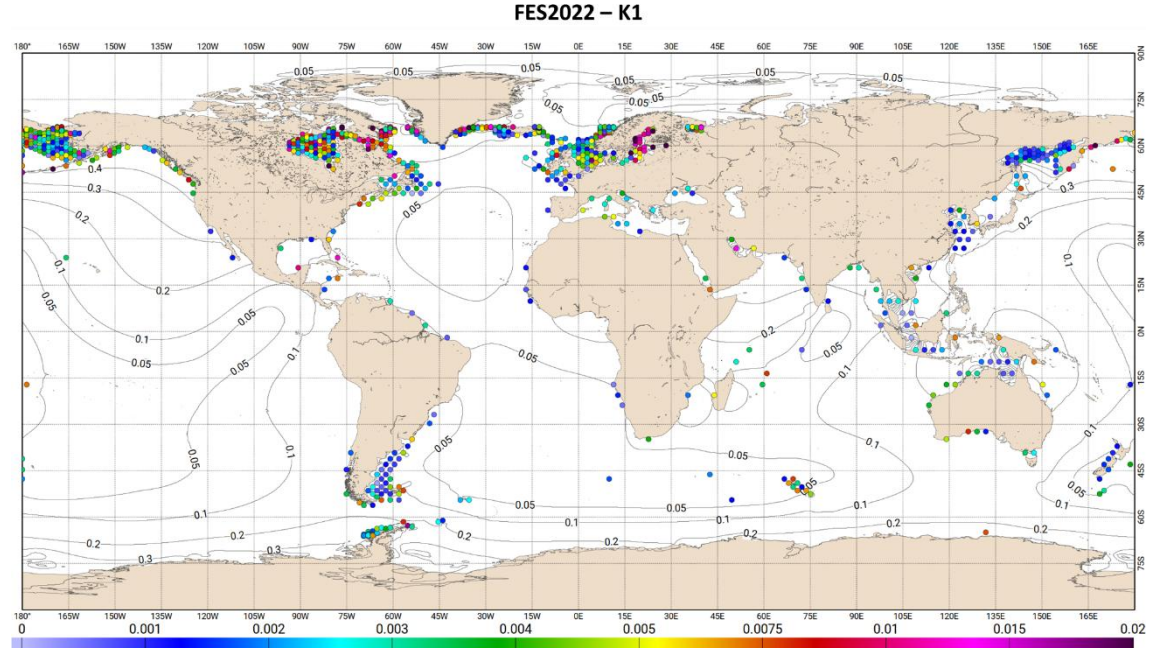
https://doi.org/10.5194/egusphere-2026-6805
Preprint. Discussion started: 11 November 2026
© Author(s) 2026. CC BY 4.0 License.

Tide gauges in all models	M2	K1	O1	S2	P1	Q1	N2	K2	M4	2N2	L2	Mu2	Nu2	J1	E2	La2	RSS
FES2014b	81.4	17.3	13.6	33.3	6.7	5.0	17.9	10.6	16.7	12.5	11.5	15.4	6.8	6.8	/	/	93.4
EOT20	86.3	19.8	15.3	37.3	7.9	5.6	19.9	12.7	16.8	12.4	/	/	/	5.4	/	/	100.6
TPXO9v5	67.6	16.9	12.1	33.8	11.2	5.4	16.9	13.4	17.1	13.9	/	/	/	/	/	/	82.2
DTU16	84.5	25.9	19.3	34.9	9.4	6.2	19.1	12.5	/	/	/	/	/	/	/	/	100.2
GOT4.10	138.0	26.5	18.7	52.4	9.1	6.3	28.8	18.5	27.3	/	/	/	/	/	/	/	155.4
FES2022 hydro	83.6	25.3	17.3	34.1	8.5	5.2	19.1	11.3	20.3	12.3	18.2	22.2	6.6	4.1	/	/	98.4
FES2022b	**31.5**	**12.8**	**9.6**	**18.0**	**5.3**	**4.7**	**10.8**	**7.1**	**9.9**	**11.1**	**9.2**	**12.9**	**4.2**	**3.8**	/	/	**42.3**

https://doi.org/10.5194/egusphere-2026-6805
Preprint. Discussion started: 11 November 2026
© Author(s) 2026. CC BY 4.0 License.



(a)



(b)

Figure B1: Vector difference (m) in color between the shelf altimetry crossover database and the FES2014b (a) and FES2022b (b) assimilated models for the K1 tidal wave. The black isolines show the K1 tide amplitude iso-contours from the models in meters.

https://doi.org/10.5194/egusphere-2026-6805
Preprint. Discussion started: 11 November 2026
© Author(s) 2026. CC BY 4.0 License.

Code and data availability

The FES2022b global tidal solution can be downloaded on the AVISO+ website: https://www.aviso.altimetry.fr/en/data/products/auxiliary-products/global-tide-fes.html. The atlas is available both on a regular cartesian grid of 1/30° resolution and on the native finite element grid.

The tidal prediction code is available here: https://github.com/CNES/aviso-fes

The T-UGOm hydrodynamic model software is available here: https://gitlab.in2p3.fr/sirocco/t-ugom (last access 9 September 2026).

The SpenOI assimilation code is available here: https://gitlab.in2p3.fr/sirocco/sirocco_spenoi (last access 9 September 2026).

The reference Delayed-Time L3 altimeter database at 1-Hz along-track resolution are distributed by the EU Copernicus Marine Service (product reference SEALEVEL_GLO_PHY_L3_MY_008_062, DOI 10.48670/moi-00146).

Author contributions

Supervision: FL and LC; paper writing, review and editing: FL, LC, EF, CS and MC, with discussions and input from all co-authors. Hydrodynamic solution: FL, EF, MC, and DG (mesh development of North-West Atlantic and Canadian northern waters); altimetry data processing: LC and MD; tide gauge data processing: EF and MC; data assimilation: EF, MC and FL; validation: LC, MD, EF, MC, RF and FL; loading and self-attraction: FL, DA;

All authors have read and agreed to the published version of the paper.

Competing interests

The authors declare that they have no conflict of interest.

Disclaimer

The authors note that the data presented in this paper are not suitable for use in navigation and disclaim all liability in the event of such use.

https://doi.org/10.5194/egusphere-2026-6805
Preprint. Discussion started: 11 November 2026
© Author(s) 2026. CC BY 4.0 License.

Acknowledgements

We want to thank CNES for the financial support to this project and also for providing the computing infrastructure (HAL) to run the model and the assimilations.

We acknowledge the SIROCCO service for providing the codes and its expertise to the project.

We thank Pascal Gégout for the computation of the Love numbers used to derive the loading and self-attraction tidal effects.

We also thank Richard Ray for his constant support in the FES2022 atlas validation process.

Financial support

The project benefited from several support funds all provided by CNES/France: purchase order n°4500066599 /DNO096 du 10.09.2020, purchase order n°4500066624 /DNO096 on 15.09.2020, purchase order n° 4500067095 / DSO091 on 15.10.2020.

References

Beaman, R.J.: High-resolution depth model for the Great Barrier Reef and Coral Sea - 100 m, Geoscience Australia, Canberra, http://dx.doi.org/10.26186/5e2f8bb629d07, 2020.

Becker, J. J., Sandwell, D. T., Smith, W. H. F., Braud, J., Binder, B., Depner, J., Fabre, D., Factor, J., Ingalls, S., Kim, S-H., Ladner, R., Marks, K., Nelson, S., Pharaoh, A., Trimmer, R., Von Rosenberg, J., Wallace, G., Weatherall, P.: Global Bathymetry and Elevation Data at 30 Arc Seconds Resolution: SRTM30_PLUS, Marine Geodesy, 32:4, 355-371, 2009.

Bennett, A. F. and McIntosh, P. C.: Open Ocean Modeling as an Inverse Problem: Tidal Theory, Journal of Physical Oceanography, 12, 1004–1018, https://doi.org/10.1175/1520-0485(1982)012<1004:OOMAAI>2.0.CO;2, 1982.

Bennett, A. F.: Inverse Methods in Physical Oceanography, Cambridge Monographs on Mechanics, Cambridge University Press, https://doi.org/10.1017/CBO9780511600807, 1992.

Caldwell, P. C., Merrifield, M. A., Thompson, P. R.: Sea level measured by tide gauges from global oceans — the Joint Archive for Sea Level holdings (NCEI Accession 0019568), Version 5.5, NOAA National Centers for Environmental Information [data set], doi:10.7289/V5V40S7W, 2015.

Cancet, M., Andersen, O. B., Lyard, F., Cotton, D., Benveniste, J.: Arctide2017, a high-resolution regional tidal model in the Arctic Ocean, ASR, V. 62, 6, 1324-1343, https://doi.org/10.1016/j.asr.2018.01.007, 2018.

https://doi.org/10.5194/egusphere-2026-6805
Preprint. Discussion started: 11 November 2026
© Author(s) 2026. CC BY 4.0 License.

Cancet, M., Fouchet, E., Sahuc, E., Lyard, F., Dibarboure, G., Picot, N.: Bathymetry improvement and high-resolution tidal modelling at regional scales, presented at the OSTST meeting in Venice, doi: 10.24400/527896/a03-2022.3304, 2022.

Cancet, M., Lyard, F. H., Fouchet, E.: Impact of sea ice friction on ocean tides in the Arctic Ocean, modelling insights at various time and space scales, Ocean Modelling, Volume 197, 102590, ISSN 1463-5003, https://doi.org/10.1016/j.ocemod.2025.102590, 2025.

Carrere, L., Busche, C., Faugère, Y., Lyard, F., Allain, D., Cheymol, C., Dibarboure, G., and Picot, N.: Tide desaliasing within a wide-swath SSO context: results with 3 WISA orbits, Ocean Surface Topography Science Team Meeting, Chicago, 2019. https://ostst.aviso.altimetry.fr/fileadmin/user_upload/tx_ausyclsseminar/files/Poster_OSTST2019_WISA_01.pdf

Carrere, L., Arbic, B. K., Dushaw, B., Egbert, G., Erofeeva, S., Lyard, F., Ray, R. D., Ubelmann, C., Zaron, E., Zhao, Z., Shriver, J. F., Buijsman, M. C., and Picot, N.: Accuracy assessment of global internal-tide models using satellite altimetry, Ocean Sci., 17, 147–180, https://doi.org/10.5194/os-17-147-2021, 2021.

Cheng, Y. and Andersen, O. B.: Towards further improving DTU global ocean tide model in shallow waters and Polar Seas, OSTST, 2017.

Egbert, G. D., and Erofeeva, S. Y.: Efficient inverse modeling of barotropic ocean tides, Journal of Atmospheric and Oceanic Technology, 19.2, 183-204, https://doi.org/10.1175/1520-0426(2002)019<0183:EIMOBO>2.0.CO;2, 2002.

EMODnet Bathymetry Consortium: EMODnet Digital Bathymetry (DTM 2020), EMODnet Bathymetry Consortium [data set], https://doi.org/10.12770/bb6a87dd-e579-4036-abe1-e649cea9881a, 2020.

EMODnet Physics - Collection of water surface height above a specific datum (SLEV) Time Series – Multi Point Time Series Observation, EMODnet [data set], https://data-erddap.emodnet-physics.eu/erddap/tabledap/ERD_EP_TS_SLEV.html

E.U. Copernicus Marine Service Information (CMEMS): Global Ocean Along Track L3 Sea Surface Heights Reprocessed 1993 Ongoing Tailored For Data Assimilation, Marine Data Store (MDS) [data set], 10.48670/moi-00146, 2022.

E.U. Copernicus Marine Service Information (CMEMS): Global Ocean Physics Reanalysis GLORYS12V1, Marine Data Store (MDS) [data set], https://doi.org/10.48670/moi-00021, 2023.

Faugère, Y., Taburet, G., Ballarotta, M., Pujol, I., Legeais, J. F., Maillard, G., Durand, C., Dagneau, Q., Lievin, M., Sanchez Roman, A., and Dibarboure, G.: DUACS DT2021: 28 years of reprocessed sea level altimetry products, EGU General Assembly 2022, Vienna, Austria, 23–27 May 2022, EGU22-7479, https://doi.org/10.5194/egusphere-egu22-7479, 2022.

GEBCO Compilation Group: GEBCO 2020 Grid [data set], doi:10.5285/a29c5465-b138-234d-e053-6c86abc040b9, 2020.

GEBCO Compilation Group: GEBCO 2025 Grid [data set], doi:10.5285/ 37c52e96-24ea-67ce-e063-7086abc05f29, 2025.

Gégout, P., Böhm, J., Wijaya, D.: Practical Numerical Computation of Love Numbers and Applications, Workshop of the COST Action ES0701, Institute of Geodesy and Geophysics, Vienna, DOI:10.13140/RG.2.1.1866.7045, 2010.

JODC: J-EGG500 Gridded Bathymetry Data, JODC [data set], https://www.jodc.go.jp/jodcweb/JDOSS/infoJEGG.html

JPL: D-109532, Revision A, SWOT Science Data Products User Handbook, Jet Propulsion Laboratory Internal Document, Pasadena, CA, 2025, https://archive.podaac.earthdata.nasa.gov/podaac-ops-cumulus-docs/web-misc/swot_mission_docs/D-109532_SWOT_UserHandbook_RevA_20250311_sig-final.pdf

https://doi.org/10.5194/egusphere-2026-6805
Preprint. Discussion started: 11 November 2026
© Author(s) 2026. CC BY 4.0 License.

Hart-Davis, M., Piccioni, G., Dettmering, D., Schwatke, C., Passaro, M., and Seitz, F.: EOT20 – A global Empirical Ocean Tide model from multi-mission satellite altimetry, SEANOE [data set], https://doi.org/10.17882/79489, 2021.

Hellerman, S., and M. Rosenstein: Normal monthly wind stress over the World Ocean with error estimates. J. Phys. Oceanogr.,13, 1093–1104, 1983.

Hersbach, H., Bell, B., Berrisford, P., Biavati, G., Horányi, A., Muñoz Sabater, J., Nicolas, J., Peubey, C., Radu, R., Rozum, I., Schepers, D., Simmons, A., Soci, C., Dee, D., Thépaut, J-N.: ERA5 hourly data on single levels from 1940 to present. Copernicus Climate Change Service (C3S) Climate Data Store (CDS) [data set], 10.24381/cds.adbb2d47, 2023.

Johnson, L. W., and Riess, R. D.: Numerical Analysis, 2nd Edition, Addison-Wesley Publishing Company, ISBN-10: 0201103923, 1982.

Kocha, C., Liévin, M., Pageot, Y., Rubin, C., Quet, V., Octau, F., Pujol, M.-I., Prandi, P., Philipps, S., Dibarboure, G., Denis, I., Nogueira Loddo, C., and Bignalet-Cazalet, F.: Three decades of sea level multi-mission satellite data reprocessed to improve mesoscale quality while ensuring climate scale consistency, Earth Syst. Sci. Data Discuss. [preprint], https://doi.org/10.5194/essd-2025-604, in review, 2026.

Le Brocq, A. M., Payne, A. J., and Vieli, A.: An improved Antarctic dataset for high resolution numerical ice sheet models (ALBMAP v1), Earth Syst. Sci. Data, 2, 247–260, https://doi.org/10.5194/essd-2-247-2010, 2010.

Le Provost, C. and Vincent, P.: Some tests of precision for a finite element model of ocean tides, Journal of Computational Physics, 65, 273–291, https://doi.org/10.1016/0021-9991(86)90209-3, 1986.

Lyard, F. H.: Data Assimilation in a Wave Equation: A Variational Representer Approach for the Grenoble Tidal Model, Journal of Computational Physics, 149, 1–31, https://doi.org/10.1006/jcph.1998.5966, 1999.

Lyard, F. H., Allain, D. J., Cancet, M., Carrère, L., and Picot, N.: FES2014 global ocean tide atlas: Design and performance. Ocean Science, 17(3), 615–649. https://doi.org/10.5194/os-17-615-2021, 2021.

Morlighem, M. et al.: IceBridge BedMachine Greenland IDBMG4, Version 3, NASA National Snow and Ice Data Center Distributed Active Archive Center [data set], https://doi.org/10.5067/2CIX82HUV88Y, 2017a. [Date Accessed 11-20-2024]

Morlighem, M., Williams, C., Rignot, E., An, L., Arndt, J. E., Bamber, J. L., Catania, G., Chauché, N., Dowdeswell, J. A., Dorschel, B., Fenty, I., Hogan, K., Howat, I., Hubbard, A., Jakobsson, M., Jordan, T. M., Kjeldsen, K. K., Millan, R., Mayer, L., Mouginot, J., Noël, B., O'Cofaigh, C., Palmer, S. J., Rysgaard, S., Seroussi, H., Siegert, M. J., Slabon, P., Straneo, F., van den Broeke, M. R., Weinrebe, W., Wood, M., and Zinglersen, K.: BedMachine v3: Complete bed topography and ocean bathymetry mapping of Greenland from multi-beam echo sounding combined with mass conservation, Geophysical Research Letters, 44, DOI: 10.1002/2017GL074954, 2017b.

Morrow, R., Fu, L.-L., Rio, M.-H., Ray, R., Prandi, P., Le Traon, P.-Y., and Benveniste, J.: Ocean Circulation from Space. Surv Geophys 44, 1243–1286, https://doi.org/10.1007/s10712-023-09778-9, 2023.

NOAA National Centers for Environmental Information, Coastal Relief Models (CRMs), NOAA National Centers for Environmental Information [data set]. https://doi.org/10.25921/5ZN5-KN44, 2023.

https://doi.org/10.5194/egusphere-2026-6805
Preprint. Discussion started: 11 November 2026
© Author(s) 2026. CC BY 4.0 License.

Ponchaut, F., Lyard, F., and Le Provost, C.: An Analysis of the Tidal Signal in the WOCE Sea Level Dataset, Journal of Atmospheric and Oceanic Technology, 18(1), 77-91, https://doi.org/10.1175/1520-0426(2001)018<0077:AAOTTS>2.0.CO;2, 2001.

Ray, R. D.: A global ocean tide model from TOPEX/POSEIDON altimetry: GOT99.2. Tech. Rep. 209478, NASA Tech. Memo., Goddard Space Flight Center, 58 pp., https://ntrs.nasa.gov/search.jsp?R=19990089548, 1999.

Schaeffer, P., Pujol, M.-I., Veillard, P., Faugere, Y., Dagneaux, Q., Dibarboure, G., and Picot, N.: The CNES CLS 2022 Mean Sea Surface: Short Wavelength Improvements from CryoSat-2 and SARAL/AltiKa High-Sampled Altimeter Data, Remote Sens., 15, 2910, https://doi.org/10.3390/rs15112910, 2023.

Schaffer, J., and Timmermann, R.: Greenland and Antarctic ice sheet topography, cavity geometry, and global bathymetry (RTopo-2), PANGAEA [data set], https://doi.org/10.1594/PANGAEA.856844, 2016.

Scott, R. B., and D.G. Furnival: A Guide to GMACMD, technical report, 2013.

Shom-IRD : MNT bathymétrique de façade de la Nouvelle-Calédonie (Projet TSUCAL), Data Shom [data set], https://dx.doi.org/10.17183/MNT_NC100m_TSUCAL_WGS84, 2021

Stammer, D., Ray, R. D., Andersen, O. B., Arbic, B. K., Bosch, W., Carrère, L., Cheng, Y., Chinn, D. S., Dushaw, B. D., Egbert, G. D., Erofeeva, S. Y., Fok, H. S., Green, J. A. M., Griffiths, S., King, M. A., Lapin, V., Lemoine, F. G., Luthcke, S. B., Lyard, F., Morison, J., Müller, M., Padman, L., Richman, J. G., Shriver, J. F., Shum, C. K., Taguchi, E., and Yi, Y.: Accuracy assessment of global barotropic ocean tide models, Rev. Geophys., 52, 243–282, https://doi.org/10.1002/2014RG000450, 2014.

Timmermann, R., Le Brocq, A., Deen, T., Domack, E., Dutrieux, P., Galton-Fenzi, B., Hellmer, H., Humbert, A., Jansen, D., Jenkins, A., Lambrecht, A., Makinson, K., Niederjasper, F., Nitsche, F., Nøst, O. A., Smedsrud, L. H., and Smith, W. H. F.: A consistent data set of Antarctic ice sheet topography, cavity geometry, and global bathymetry, Earth Syst. Sci. Data, 2, 261–273, doi:10.5194/essd-2-261-2010, 2010.

Tozer, B, Sandwell, D. T., Smith, W. H. F., Olson, C., Beale, J. R., and Wessel, P.: Global bathymetry and topography at 15 arc sec: SRTM15+, OpenTopography [data set], https://doi.org/10.5069/G92R3PT9, 2019 [Accessed: 2024-11-20]

Weatherall, P., Marks, K. M., Jakobsson, M., Schmitt, T., Tani, S., Arndt, J. E., Rovere, M., Chayes, D., Ferrini, V. and Wigley, R.: A New Digital Bathymetric Model of the World's Oceans, Earth and Space Science, 2, doi: 10.1002/2015EA000107, 2015

Wessel, P., and W. H. F. Smith: A global, self-consistent, hierarchical, high-resolution shoreline database, J. Geophys. Res., 101(B4), 8741–8743, doi:10.1029/96JB00104, 1996.

Zaron, E. D. and Elipot, S.: An Assessment of Global Ocean Barotropic Tide Models Using Geodetic Mission Altimetry and Surface Drifters, J. Phys. Oceanogr., 51, 63–82, https://doi.org/10.1175/JPO-D-20-0089.1, 2020.

Zawadzki, L., Ablain, M., Carrere, L, Ray, R. D., Zelensky, N., Lyard, F., Guillot, A. and Picot, N.: Investigating the 59-Day Error Signal in the Mean Sea Level Derived From TOPEX/Poseidon, Jason-1, and Jason-2 Data With FES and GOT Ocean Tide Models. IEEE Transactions on Geoscience and Remote Sensing. 56. 3244-3255. 10.1109/TGRS.2018.2796630, 2018.